A comparative study of platinum nanodeposits on HOPG (0001), MnO(100) and MnOx/MnO(100) surfaces by STM and AFM after heat treatment in UHV, O2 , CO and H2

Tsybukh, R.

CHAPTER 4

Platinum deposition on HOPG

The morphology of platinum nanodeposits prepared by physical vapor deposition in UHV on a HOPG surface was analyzed using STM. After deposition STM images showed a random distribution of irregularly shaped three-dimensional platinum particles with an apparent average height of 0.2-0.3 nm. Annealing of the Pt/HOPG system in UHV at 500 °C for 7 h resulted in a very narrow size distribution of the platinum particles with an apparent average height of 0.4-0.6 nm. The annealing of the system up to 500 °C in the presence of O_2, H_2 and CO at a pressure of 2.0×10^{-5} mbar transforms the deposits into round particles with an apparent height of 0.4-1.4 nm. The most pronounced effect was observed upon heating in the presence of CO. STM imaging just after platinum deposition revealed a small decoration of the substrate steps with Pt particles that increased after subsequent temperature treatment of the system in UHV. The presence of the gaseous atmospheres distinctly enhanced this effect.

The experiments indicate that the growth of Pt nanoparticles occurs according to the coalescence mechanism in UHV as well as in gaseous environment (H_2, CO, and O_2).

4.1 Lattice structure of HOPG

The crystal lattice of highly oriented pyrolytic graphite consists of an ordered stacking of basal planes where carbon atoms within the planes form hexagons. In the planes each carbon atom is trigonally bonded to the three nearest neighbors by means of sp^2 hybridized orbitals, which take part in the formation of strong covalent C-C (σ) bonds. The overlap of unhybridized $2p_z$ orbitals from each carbon atom additionally leads to the formation of π bonds. The interaction between the basal planes is largely dominated by van der Waals interaction. The basal planes are stacked in the sequence ABAB. The surface structure of the HOPG(0001) surface is presented in Fig. 4.1.

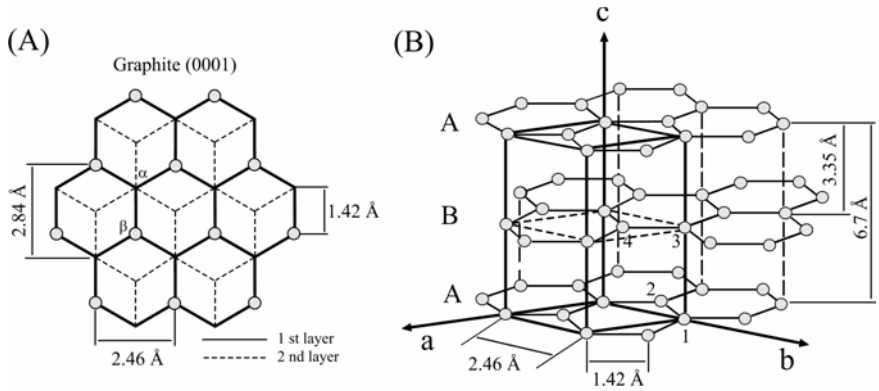

Figure 4.1: ***(A)*** *Schematic representation of two successive layers of HOPG (top view).* ***(B)*** *Side view of HOPG structure. The unit cell of the HOPG indicated by the black solid lines has four different carbon atoms marked 1, 2, 3 and 4. Note: the atoms in a HOPG layer are designated as either α or β sites, depending on whether or not a given carbon atom has an atom below or above it in adjacent planes. β atoms have no carbon atom directly below or above them and have been shown to be the carbon atoms that appear usually in STM images of the surface while α atoms do have such neighbors. The in plane nearest-neighbor distance (from C centre to C centre) in a HOPG layer is 1.42 Å, but the β-β distance is 2.46 Å [1].*

4.2 Literature review

4.2.1 Platinum deposition on HOPG

The use of well-defined and easily prepared substrates greatly reduces the amount of work associated with their characterization prior to usage in model supported metal catalysts studies. Highly oriented pyrolytic graphite perfectly matches such requirements. Of value also is that among a range of similar substrates it has a relatively simple structure. In addition, it is conductive and chemically "inert". The latter property may provide additional benefits for the analysis of the catalytic properties of a supported phase.

An extensive list of studies on the deposition of various elements on a HOPG surface performed by a range of methods is already available [2-77]. Platinum deposits on a HOPG surface were intensively studied with scanning probe microscopy (SPM) in the 1990s [3, 5, 7-17, 21, 22, 42, 43, 45, 46, 49-52] and in some more recent reports [56, 57, 59, 63, 65, 73-76] as well. It should be noted that imaging of deposited materials on this surface with SPM techniques is not an easy task. Detailed analysis of the size distribution profiles of deposits and specific morphological features in many early SPM studies was not accomplished due to

the lack of resolution. This can be explained partly by difficulties of the SPM imaging because of weak adhesion and mobility of deposits on HOPG.

Concerning the influence of gas environment on the size and morphology of Pt deposits on HOPG by using STM useful observations have been made in [13-15, 22]. However, these reports mainly dealt with the analysis of a pretreatment action of some gases on the Pt/HOPG system. Only a few reports [21, 27] have been dedicated to the characterization of the morphology of finely dispersed Pt on this substrate after contact with gas mixtures. Thus, a clear correlation between the structure of deposits and their activity in chemical reactions has not been established. Today, the situation does begin to change. For example, recent study by Bayati *et al.* [73] demonstrated that the reactivity of Pt nanoparticles deposited on HOPG for electro-oxidation of CO and methanol decreases with decreasing particle size. In [74, 75] the H_2–D_2 exchange reaction has been investigated on the Pt/HOPG system. A clear dependence of the reaction on the morphology of Pt deposits has been found: flat monolayer clusters of Pt exhibited higher catalytic activity at high pressures (24 Torr) than taller Pt clusters. It is worth noting that beside Pt other metals supported on HOPG are actively studied. For instance, recently catalytic tests on CO interaction with silver [67] and gold [68] nanoparticles as well as thin films of these metals on HOPG and oxidized with atomic oxygen under UHV were performed. Also silver nanoparticles supported on HOPG in a range of coverages have been tested toward the adsorption of O_2, $CHCl_3$, and CCl_4 [77]. Finally, the investigations of different bimetallic Pt containing nanoparticles prepared on HOPG are in progress [78-80].

Depending on the deposition conditions and precursors, platinum deposits on a HOPG surface exhibit different morphologies and behavior. Chemical impregnation methods [17, 24, 30] generally produce less evenly sized deposits than vacuum vapor deposition methods [14, 17, 19, 25, 55] and deposition techniques based on mass selection of clusters from a cluster beam [36, 43, 44].

As mentioned above there are considerable difficulties of SPM imaging of the detailed structure of deposits on HOPG, and to the author's knowledge unambiguously atomic resolution of the external surface of noble metal nanodeposits on HOPG has only been achieved by Humbert *et al.* [6] for Pd and Atamny and Baiker [46] for Pt. In the former case 1.5 nm large Pd clusters imaged in air were found to have a tetrahedral shape with (111) facets and were epitaxially oriented: Pd(111)//graphite(0001), Pd($11\bar{2}$)//graphite(0100). In the latter case quite large 2D Pt particles exhibited the same symmetry as the surface implying a (111) orientation of Pt. Atomic resolution of the particle's edge, however, could not be achieved as stated due to the organic contamination originating from the solution.

4.2.2 Interaction of O_2, CO and H_2 with Pt clusters

Carbon monoxide, hydrogen and oxygen are widely used as probe molecules to determine the metal surface area and dispersion of the supported catalysts [81-87]. The fist two molecules are used most frequently. Besides that CO is often used as a probe molecule since the intramolecular C-O stretch vibration is very sensitive to the local adsorption geometry and the presence of neighboring adsorbates [88-90]. Carbon monoxide adsorption on Pt is non-dissociative and non-activated and it adsorbs predominantly in the linear form on extended Pt surfaces as well as nanoparticles [87, 91, 92]. At ambient temperatures the stoichiometry is assumed to be 1:1 for sufficiently high pressure (Torr range) [82, 85]. On-top CO is the only species observed on the Pt(111) surface between 160 and 400 K, independent of gas pressure (10^{-7}-500 mbar) [93]. The latest studies revealed that CO binds exclusively atop of tiny (sub-nanometer) Pt clusters containing between 3 and 22 atoms [94]. It is worth noting that under 40 Torr CO was found to dissociate on Pt(111), Pt(557) and Pt(100) single crystals at 673, 548 and 500 K, respectively [95]. As well Park *et al.* [96] have found that CO adsorbs molecularly and dissociates upon heating on the Pt(410) surface. CO desorbs in 5 peaks at 550, 500, 450, 380 and about 130 K from this surface.

Both H_2 and O_2 dissociate at room temperature on Pt particles and require a pair of adjacent Pt atoms. The measurements imply an adsorption stoichiometry 1:1 for counting the number of Pt surface sites. However, this implication may not always hold. For example, for oxygen a ratio of O/Pt=0.71 have been reported [83]. As well, recent chemisorption experiments on Pt particles with sizes ranging from 0.98 to 1.26 nm [86] revealed that hydrogen coverage depends strongly on the support ionicity and the H/Pt ratio may be higher than unity. It is worth mentioning that Tsuchiya *et al.* [97] registered at least four different states of chemisorbed H_2 on a platinum black catalyst with peak maxima at about –100, –20, 90, and 300 ° C.

Whereas the adsorption of H_2, O_2 and CO on different Pt single crystal surfaces has been studied extensively, the details of the interaction of these molecules with tiny metal clusters have not been yet studied thoroughly. For tiny clusters consisting of several metal atoms theoretical quantum mechanical calculations are almost the only sources of investigation [98]. As already discussed in § 3, small metal particles/clusters exhibit novel chemical and physical properties, due to the presence of less coordinated atoms (such as on corners and edges) than in the bulk. This implies that the interaction between a molecule and a metal cluster is significantly different from the interaction with a bulk metal surface. Important questions are how a molecule is attached to a metal cluster and does it dissociate or does it remain intact. An excellent example in this context

represents the latest remarkable result due to Vajda *et al.* [99] who by quantum chemical calculations as well as experimental studies [100] demonstrated that size-preselected Pt clusters with 8-10 atoms stabilized on high-surface-area supports are 40-100 times more active for the oxidative dehydrogenation of propane than previously studied platinum and vanadia catalysts, while at the same time maintaining high selectivity towards formation of propylene. It was established that under-coordination of the Pt atoms in the clusters is responsible for the higher reactivity compared with extended surfaces. In the following some recent advances in the study of the interaction of free and supported Pt clusters on HOPG and some other substrates with CO, H_2 and O_2 are shortly reviewed.

According to MD simulations performed by Wu and Chan [101], oxygen (equilibrated at 250 and 298 K) on Pt clusters supported on graphite adsorbs primarily on the interstitial sites of Pt and the interaction energy between oxygen and Pt is claimed to be strong, especially for large clusters. Li and Balbuena [102] using DFT computations to study the interaction between atomic and molecular oxygen with isolated small Pt_n clusters (n=2-6) established that the adsorption energy for atomic oxygen strongly depends on the metal cluster size and geometry. The dependence of the activation barrier for dissociation of adsorbed O_2 on the Pt cluster size was calculated. For instance, the adsorption energy of the oxygen molecule on the Pt_5 cluster was found to be 0.53 eV. The most recent DFT calculations carried out by Xu *et al.* [103] concerning the effect of cluster size on the reactivity of small Pt_x clusters (x=1-5 and 10) toward the oxidation of CO pointed to a large enhancement of the binding of all the adsorbed species compared to the binding on Pt(111), particularly on Pt_{1-5}. In the range $x \leq 5$ substantial size-dependent variations in binding energy were found. Whereas the binding energies of oxygen reach a minimum (strongest adsorption) at Pt_{4-5}, those of CO rise with increasing cluster size. The binding strength of these adsorbates generally follows the order $O>CO>O_2$ over the entire range of Pt particle sizes. The overall trend is that the binding energies of all the species become more positive and converge toward the bulk levels with increasing particle size. The binding energies of all the species on Pt_{10} have already approached the Pt(111) levels. It was shown that atomic O and CO prefers binding to a single Pt atom, regardless of the availability of two-and three-fold sites (except for Pt_2-CO). Oxygen atoms consistently bind to the apexes of the Pt clusters. Adsorption occurs without significant structural modification of the Pt_x clusters and with a nearly uniform 0.6-0.7 electron charge transfer from the clusters to the O atoms. The O binding energy varies non-linearly with cluster size and is lower than the binding energy on Pt(111) in all cases with the exception of Pt_{10}. The maximum binding energy for O occurs at Pt_5, that is 0.7 eV stronger than Pt(111)-O (-1.2 eV). For O_2 the maximum interaction is observed at Pt_4 (-2.5 eV) compared to Pt(111)-O_2 (-0.6

eV). O_2 adsorption is particularly strong on Pt_4 and Pt_5, where it transforms tetrahedral Pt_4 into a square and trigonal bipyramidal Pt_5 into a square pyramid. The authors claim that under ambient and typical oxidation catalysis conditions, the prevailing compositions are expected to be between Pt_xO_x and Pt_xO_{2x}. These clusters are found to be distinct from the bulk oxides and prefer 1-D and 2-D chain and ring-like shapes.

Carbon monoxide interaction decreases monotonically with cluster size from -3.5 eV for Pt_1 to -2.0 eV for Pt_{10}, that is close to the binding energy of CO with the Pt (111) surface (-1.8 eV). As in the case of adsorption on large Pt surfaces CO, binds to the small Pt clusters according to the Blyholder scheme [104]. CO is predicted to bind through its C atom in linear conformations, except on Pt_2. The preference for a bridge site is unique to Pt_2 and is 0.7 eV more stable than the linear binding state.

In earlier experiments by Heiz *et al.* [105] it was observed that CO desorbed from monodispersed Pt_1, Pt_2 and Pt_3 clusters deposited on an atomically clean silica thin film in a distinct peak centered at 340 K with an activation energy of about 64 kJ/mol. It was shown that this state is a unique feature of highly dispersed Pt on SiO_2. CO desorption from other Pt sites was also detected, exhibiting higher desorption activation energies, but the nature of these sites has not been determined. In the recent investigation by Nakamura *et al.* [75] by TPD measurements of CO from Pt deposited on HOPG with Pt coverage of 0.12, 0.18, and 0.24 (the majority of Pt clusters were of 1-2 atoms in height and 1.5 - 4 nm in width) two desorption peaks of CO at *ca.* 300 and 450 K were registered. The latter peak was assigned as the CO desorption from the Pt surface which has the same property as single crystal surface. The peak at 300 K has not been reported before and it was concluded that some of the Pt particles deposited on HOPG have quite different catalytic properties than the Pt single crystal surface. This behavior was ascribed to the interface interaction between Pt particles and HOPG.

Ganteför *et al.* [106] also found good agreement with the Blyholder model for CO chemisorption on Pt_n (n=1-4) clusters. The strength of the π-backdonation is found to be larger for small particles compared to the corresponding single crystal surfaces. Curiously, recent DFT calculations [107] revealed an unexpected interaction of CO with Pt clusters consisting of a few atoms: CO can adsorb upside-down (the O atom close to the metal atom) on small Pt_mAu_n clusters (m, n=0-4) contrary to the bulk surfaces such as Pt(111), Au(111), and $Pt_{0.25}Au_{0.75}$(111). The authors claim that CO upside-down adsorption on pure Pt clusters may be detected using FTIR spectroscopy. Finally, concerning CO adsorption on small Pt clusters it is worth mentioning the DFT computations by Yourdshahyan *et al.* [108] which revealed substantially stronger CO chemisorption energy to Pt_3 nanocluster (3.92 eV) deposited on alumina compared to the bulk Pt (1.70 eV).

According to the recent DFT calculations performed by Zhou *et al.* [109] concerning dissociative chemisorption of hydrogen and sequential H desorption for selected Pt_n (n = 2-5, 7-9) clusters the reaction processes are driven by charge transfer from Pt atoms to H atoms assisted by strong orbital overlap between Pt 5d orbitals and H 1s orbital, which leads to electron delocalization in large clusters of metal hydrides. The calculations established that the number of H atoms chemisorbed on the small Pt clusters increases almost linearly as the cluster size increases. But even tiny Pt clusters can accommodate a considerable amount of hydrogen, e.g., Pt_2 can accommodate up to 12, and Pt_9 up to 34 H atoms.

Finally, it is worth to mention that hydrogen at low coverages was found to adsorb on supported Pt clusters on basic substrates in the platinum 3-fold hollow sites near cluster edges at high temperatures, whereas in the case of acidic supports, the H appears to adsorb at the Pt cluster edge atop sites [110]. At higher coverage, the H prefers the 3-fold hollow sites with approximately equal bond strength on both acidic and basic support.

4.3 Pt/HOPG model system: experimental results of annealing in UHV and in atmospheres of O_2, CO and H_2

The sintering of metal nanoparticles on different model supports is an important and very active research area that has an objective to answer the important question: how the deactivation of the real supported catalysts occurs under operating conditions [111]?

This section presents the results of STM imaging of a HOPG (0001) surface after deposition of Pt and subsequent annealing in UHV and in the presence of oxygen, carbon monoxide and hydrogen.

The HOPG substrates used were 1 cm^2 and 1 mm thick and prepared by cleaving in air using adhesive tape. Prior to the Pt deposition the HOPG surfaces were treated according to the procedure described in § 2.9.1.

In most cases STM and AFM images of the HOPG surface yield only every other atom with the in-plane lattice constant of 2.46 Å, and its full honeycomb structure revealing all six carbon atoms of each hexagon can only be obtained under certain conditions [112]. Despite the fact that the HOPG surface was imaged with atomic resolution at the beginning of the era of SPM [112], there are still several models explaining its observed surface structure [113, 114]. The question which one is correct remains even today unanswered [114].

All STM experiments conducted in the present study registered the HOPG surface having a honeycomb structure with the in-plane lattice constant of 2.46 Å (Fig. 4.2).

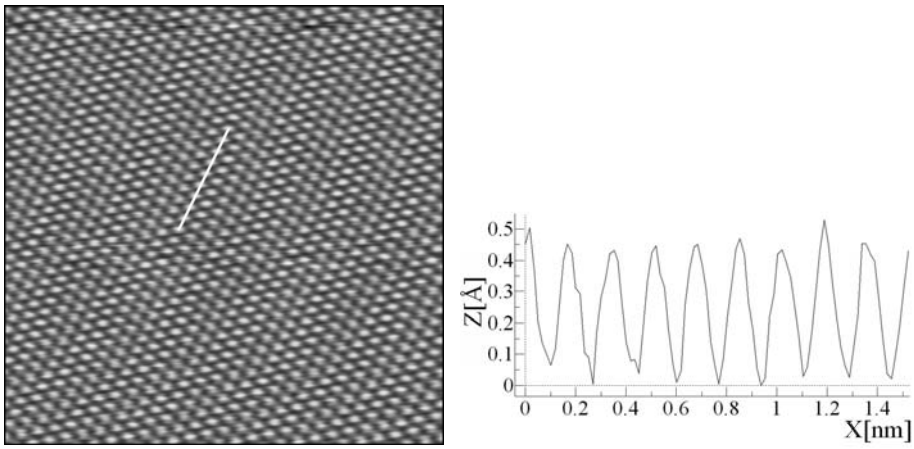

Figure 4.2: *STM image (6 × 6 nm²) of the HOPG(0001) surface (U_t = 0.5 V, I_t=0.2 nA). The image has been enhanced by filtering. The line-profile, whose position is marked with the white line on the image, shows the apparent atomic corrugation.*

4.3.1 Pt on HOPG surface. Annealing in vacuum

Metal depositions on van-der-Waals substrates like HOPG generally lead to regular shaped islands [115]. In general, in the absence of surface defects, cluster growth is determined by temperature and evaporation rate. By controlling these parameters one can control the island density and size. Growth processes can be well described by nucleation of atoms once nuclei of a critical size have been reached. Theoretical description and rate equations of these processes are given in [116, 117 and ref. therein].

In order to get an idea what kind of structures Pt deposits can form on HOPG under our experimental deposition conditions, samples with several monolayers (5 ML) and a sub-monolayer (~ 0.05 ML) Pt coverage were prepared. An STM image of the Pt (5 ML)/HOPG sample is shown in Fig. 4.3 (A).

The amount of the deposited material was checked by means of RBS (Fig. 4.4). As can be seen, the deposition of 5 ML of Pt produced a uniform and continuous though rough sponge-like Pt film on the HOPG surface with some crevice-like voids. The apparent height of the film as determined from the STM line-profile is around 0.8 nm [Fig. 4.3 (A)]. STM images of the second sample (~ 0.05 ML Pt) showed irregularly shaped 2-D/3-D clusters. The clusters are spread randomly over the surface and they have an average apparent height of 0.2-0.3 nm, i.e. 1 ML (Fig. 4.5). A rough estimation based on the assumption of Pt(111) island and taking into account the model of atom arrangement within a cluster, discussed in § 3.3 leads to up to 10-15 atoms in such a cluster.

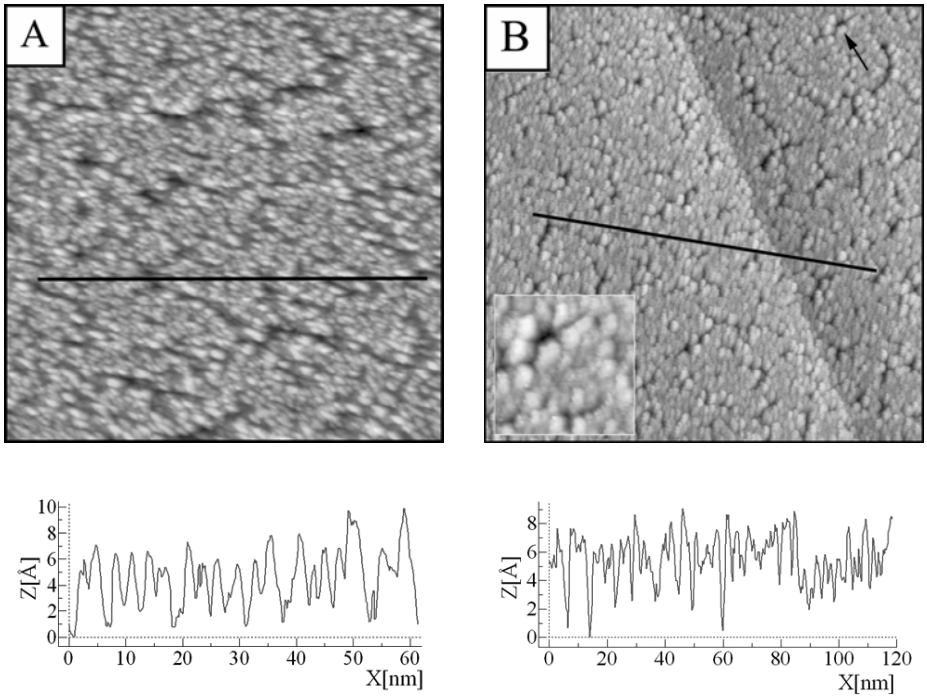

Figure 4.3: ***(A)*** *STM image (70 × 70 nm²) of 5 ML thick Pt film on HOPG and a line profile through the surface.* ***(B)*** *STM image (150 × 150 nm²) of the same sample after annealing in UHV at 500 °C for 1 h and a line profile through the surface. The arrow on the image marks the location of the surface shown on the inset (20.1 × 20.1 nm²). Imaging conditions:* ***(A)*** U_t *= 0.7 V,* I_t*=0.2 nA,* ***(B)*** U_t*= - 0.7 V,* I_t*= 0.3 nA.*

To investigate the influence of temperature on the Pt deposits each sample was annealed at 500 °C in UHV for 1.5 h. After such a treatment the Pt film on the first sample appeared to be more structured, that was manifested in a much better contrast of the STM images [Fig. 4.3 (B)]. As the inset in Fig. 4.3 (B) shows, there are some patches of hexagonal-like arrangement of the Pt deposits on the substrate, especially in the regions of the surface around the voids. Apparently, the annealing causes Pt atoms and clusters to diffuse on the HOPG surface and they subsequently arrange in the most energetically favorable (with a minimum exposed surface/volume ratio) surface structures (agglomerates). At the same time the Fourier transform (not shown) of the STM images did not indicate a long range order of the Pt film either before or after the annealing. A schematic arrangement of an agglomerate assembled from several Pt clusters consisting of 13 Pt atoms (Pt_{13} - the first "magic number" for a free cluster, see § 3. 3) along with some separate clusters of smaller size is illustrated in Fig. 4.6. Interestingly, recent AFM study [118] revealed that the shape transformation and the coalescence in preferred directions for the Pt nanosheets with a uniform thickness of *ca*. 3.5 nm

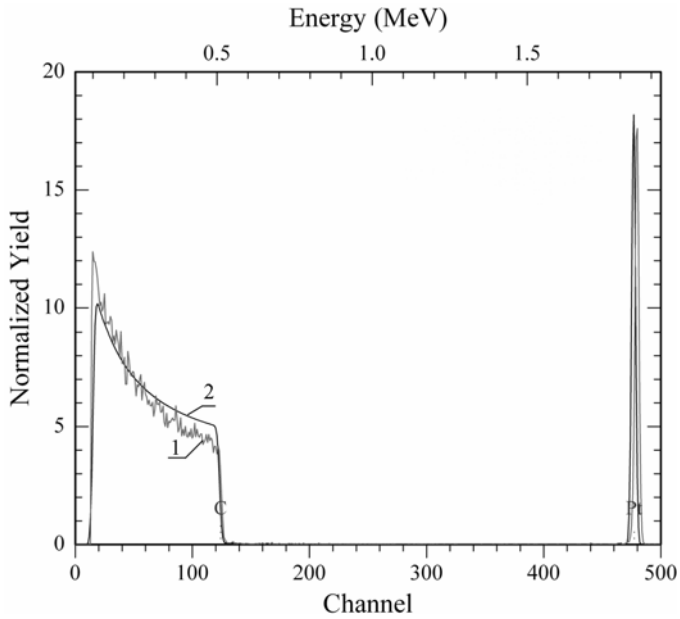

Figure 4.4: *RBS spectrum of a 5 ML thick Pt layer deposited on HOPG. The measurement was done with 2.0 MeV $^4He^+$ and a detector at a scattering angle of 165°. The channel numbers of C and Pt on the surface are as indicated. The measured spectrum (1) and the fit (2) calculated by the RUMP program.*

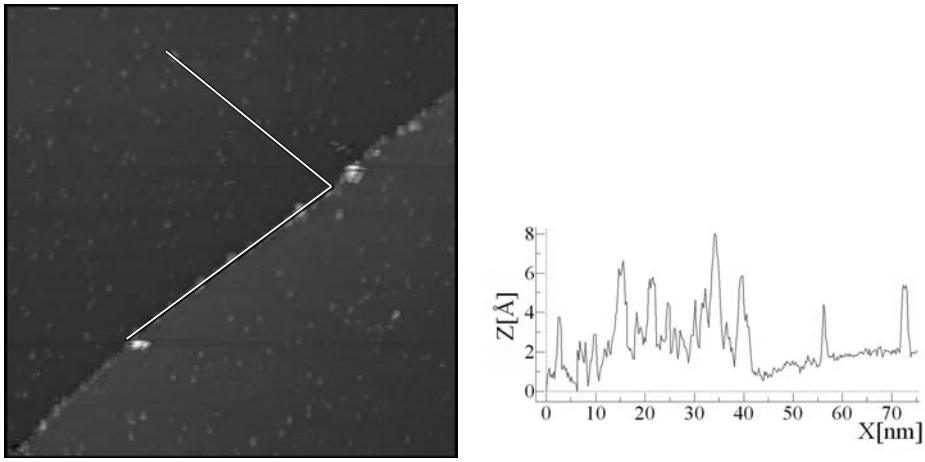

Figure 4.5: *STM image (70 × 70 nm²) of the HOPG(0001) surface with ~ 0.05 ML of Pt and a line-profile along a step and a terrace. Imaging conditions: U_t= 0.2 V, I_t = 0.1 nA.*

supported on graphite even at room temperature. This was attributed to the high surface energy for the edge parts of Pt nanosheets.

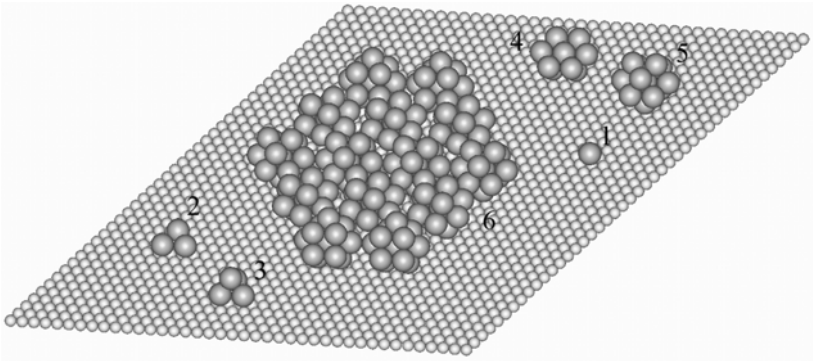

Figure 4.6: *Real space model of Pt clusters on a HOPG surface:* ***(1)*** *platinum monomer,* ***(2)*** *trimer (P_3),* ***(3)*** *tetramer (P_4),* ***(4)*** *decamer (P_{10}) and* ***(5)*** *Pt_{13} "magic number" cluster are shown. Clusters are shown with the atomic radii of the Pt atoms. For illustrating purposes an imaginary agglomerate* ***(6)*** *consisting of several Pt_{13} clusters is depicted.*

Concerning the issue of Pt particles arrangement on HOPG it should be noted that the lattice mismatch between Pt (the room temperature lattice constant of Pt, a=3.92 Å [119]) and HOPG is ~ 59 %. However, there is a possibility that some deposited clusters orient to the substrate with their close-packed Pt(111) surfaces which have an in-plane lattice constant of 2.77 Å [119], in this case the lattice mismatch is reduced to ~ 13 %. The possibility of such Pt particles arrangement is supported by the findings of Clark and Kesmodel [16] that are based on high resolution image analyses of Pt deposits for coverages of 5-30 % of a monolayer. These workers found that two-dimensional Pt islands on HOPG exist as a hexagonal close packed (hcp) array. The epitaxial arrangement of Pd and Pt particles on this surface was also registered by Humbert *et al.* [6] and Atamny and Baiker [46], respectively. These results are in agreement with very recent MD studies performed by Ryu *et al.* [120] according to which Pt clusters supported on graphite may have a hexagonal or a rectangular lattice as well as mixed lattice in the bottom layer.

There are several possibilities for a single Pt atom to be adsorbed on the HOPG surface. This subject was analyzed in [7] and the probability of a Pt-atom to bind on the different HOPG surface sites: α, β, hollow-site and in-between sites, was determined. The adsorption probability near a β-site appeared to be slightly higher (a factor of 2) than near a hollow-site or an α-site. A 26.4 % probability was found that the atom sits in-between sites. The authors claimed to observe Pt_2-dimers and Pt_3-trimers by STM. Because of the very broad distribution of Pt-dimer bond length (from 1.8 to 2.9 Å) with an average value of 2.45 Å it was proposed that the bond length is not related to the graphite lattice distance. Two kinds of adsorbed Pt-trimers on HOPG surface were found, either linear chains or

equilateral triangles with an average bond length of 2.66 ± 0.32 Å. It should be noted that for the gas phase Pt_2 and Pt_3 the corresponding bond distance was calculated to be 2.39 and 2.34 Å, respectively [121]. According to a more recent study [76], Pt (deposited on HOPG by physical vapor deposition) atoms locate on the β-sites of the HOPG surface. This indicates ~ 13 % shrinking of Pt-Pt distance compared to the bulk Pt-Pt nearest-neighbor distance of 2.77 Å.

The line-profiles through the STM images of Pt (5 ML)/HOPG sample before and after annealing taken with a sample bias of 0.7 V and - 0.7 V (Fig. 4.3) showed that the apparent height of the Pt film was not influenced by the bias voltage change. There is also a good correlation between the apparent heights of Pt deposits determined by STM and the thickness of the film obtained by RBS measurements. The sample with ~ 0.05 ML Pt annealed under identical conditions exhibited particles with an apparent height in the range of 0.4 -1.2 nm decorating the substrate steps along with a small amount of particles with an apparent height of about 0.2-0.3 nm located on the terraces (Fig. 4.7).

In Fig. 4.8 the typical particle height distribution along one of the substrate steps is shown. It is interesting to note that the height of Pt particles along the steps is quantized by steps of ~ 0.1 nm. The exact nature of this phenomenon is not clear at the moment. Probably this observation reflects the size-dependent stability of these particles and apparently they grow by increasing the number of shells in the particle. In view of the detection of Pt particles of discrete size in our studies and the importance of stability of clusters on surfaces in heterogeneous

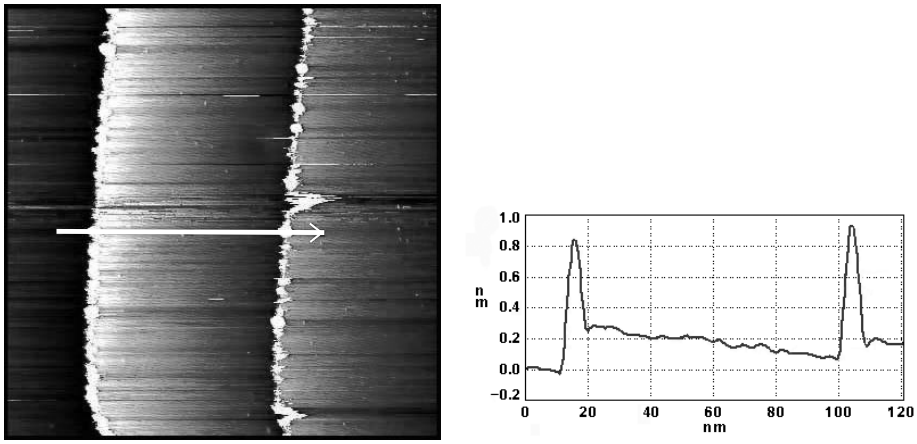

Figure 4.7: *STM image (200 × 200 nm²) of HOPG with deposited ~ 0.05 ML Pt after annealing in UHV at 500 °C for 1.5 h showing two monoatomic steps decorated with Pt particles. Aside of the image, a line-profile, whose position is marked with the white line on the image, shows the apparent height of the particles situated near neighboring step edges. Imaging conditions: U_t = 0.2 V, I_t =0.2 nA.*

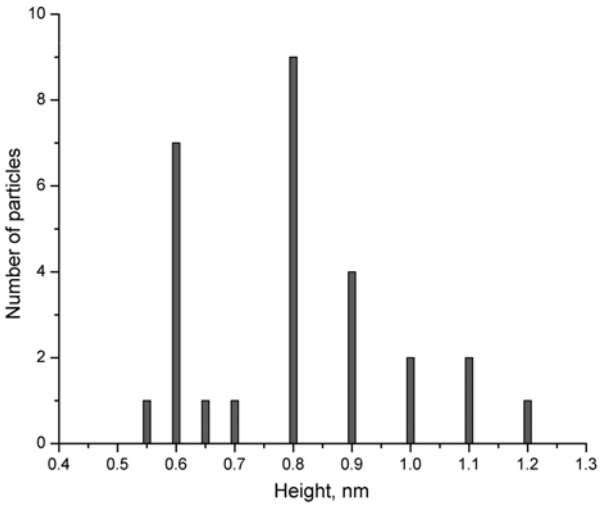

Figure 4.8: *Histogram of the apparent height of the Pt particles obtained by analyzing of the STM image along one of the steps presented in Fig. 4.7. Here the height is the sum of the height of the monoatomic step and the apparent height of the particle.*

catalysis this issue will be considered in more detail in the Discussion.

Since neither a high nor a very low coverage do not allow to observe changes that may occur with Pt particles with plausible statistics, Pt/HOPG samples up to a total coverage of 0.2-0.4 ML of bulk mass Pt equivalent were prepared, which exhibit a sufficient interparticle distance and the particle size is small. It is worth to note that when STM imaging was carried out with a rather large tunneling current (0.5 - several nA), it was found that Pt particles could be displaced by the STM tip from their original position. This implies very weak interaction with the support. An example of such an event is shown in Fig. 4.9. To avoid this to happen, the experiments were carried out with a tunneling current of 0.1-0.3 nA and a bias voltage of 0.2-0.5 V. In this range of tunneling conditions no change in the apparent height of the clusters was observed.

The STM image after supply of 0.3 ML of Pt on an HOPG is shown in Fig. 4.10 (A). Initially, Pt deposits were randomly distributed over the surface along with a small amount of particles pinned to the steps of the substrate. These pinned particles also had certain discrete sizes. But, since it was not possible to visualize the external surface of the particles, i.e. their geometric shape, it could not be determined whether these particles belong to “magic numbers”.

The obtained height distribution is shown in Fig. 4.10 (B), yielding the average apparent height of the particles in the range of 0.25-0.3 nm. The Pt deposits had an irregular particle-like morphology and were fitted best by using a lognormal distribution probability function, as displayed in Fig. 4.10 (B).

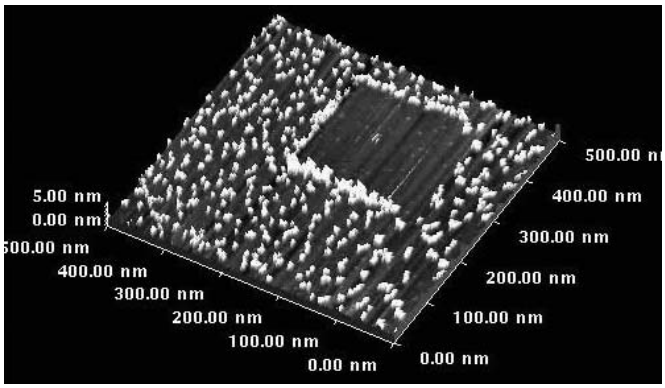

Figure 4.9: *STM image (500 × 500 nm²) of Pt/HOPG showing an example of the relocation of Pt particles by a tip at high tunneling current. Imaging conditions: U_t=0.5 V, I_t=2 nA.*

In should be noted that the size (height) distribution in all of the experiments performed in the present work was determined from a series of STM images by taking line profiles across each of the particles. Although this method of analysis is very time consuming, it resulted in much more accurate measurements in comparison to the application of automatic size determination by specialized software, because it was not always possible to get rid of occasional strong deterioration of the STM images by noise.

Further a Pt/HOPG sample with 0.3 ML Pt was heat-treated first in UHV at 500 °C for 1.5 h and then under identical conditions for a longer time (7 h in total). After the first annealing step, the shape, the density and the size distribution of Pt particles had not changed significantly and the average particle height remained within the range of 0.2-0.3 nm. A small part of larger particles was observed along the step edges of the substrate. After longer annealing, the density of the particles on substrate's surface free of steps decreased, and the average particle height increased to 0.5-0.6 nm [Fig. 4.11 (B)]. On some locations of the surface irregularly shaped agglomerates were observed consisting of several separate round particles.

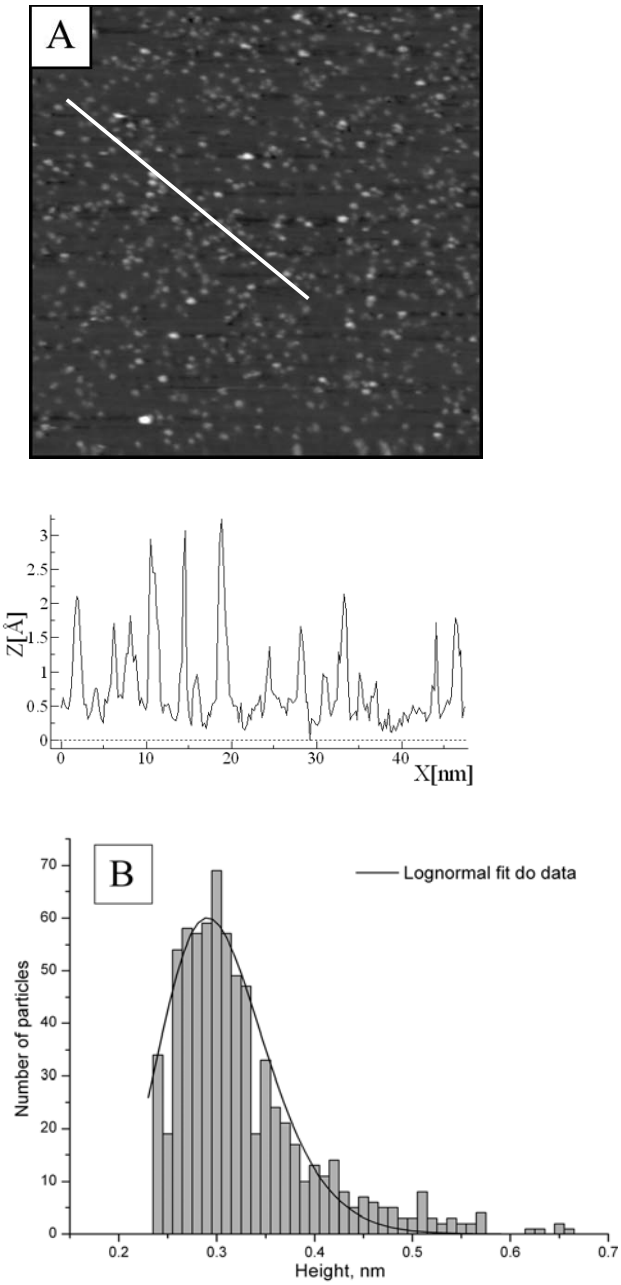

Figure 4.10: ***(A)*** *STM-image (70 × 70 nm²) of 0.3 ML of Pt on HOPG and corresponding height distribution of the Pt particles* ***(B)****.*

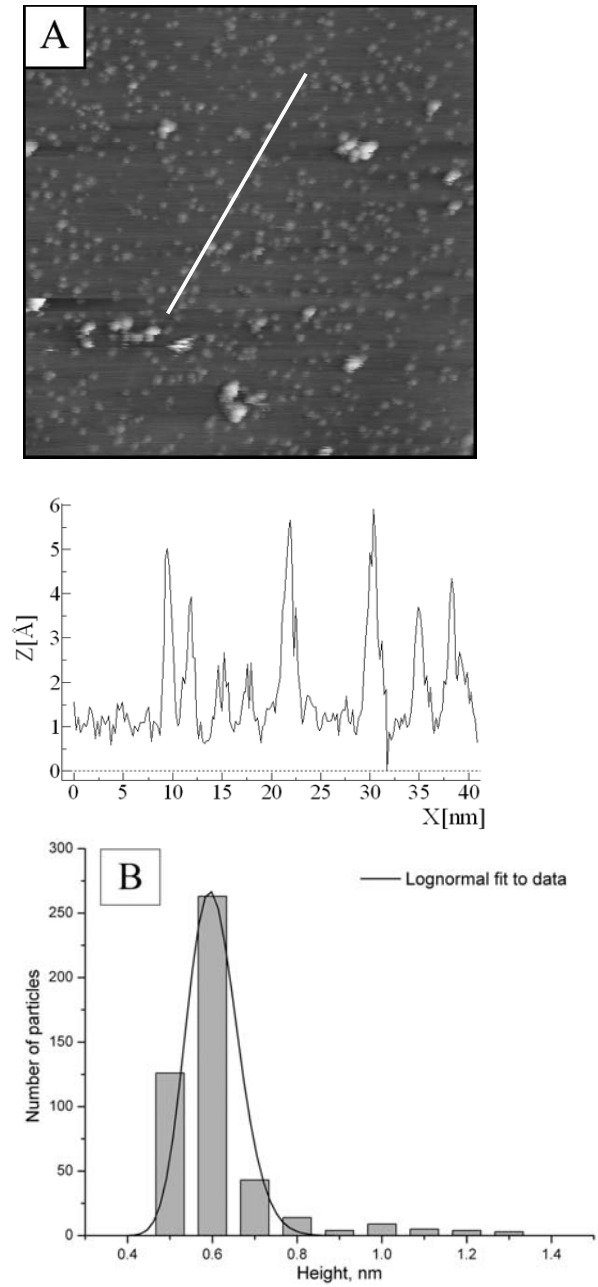

Figure 4.11: ***(A)*** *STM-image (70 × 70 nm²) of a Pt/HOPG sample with 0.3 ML Pt after annealing in UHV for 7 h at 500 °C.* ***(B)*** *Height distribution histogram of Pt particles on the same sample measured from multiple STM images taken on different sample locations. Particles within a range of heights ± 0.03 nm from the indicated values are grouped together.*

4.3.2 Annealing in oxygen

In the next set of experiments 0.2 ML of Pt was deposited on HOPG and subsequently heated in oxygen $p(O_2)=2\times10^{-5}$ mbar at 500 °C for 1 h. Figure 4.12 (A) shows the sample surface before annealing in oxygen and Fig. 4.12 (B) illustrates the height distribution of the Pt particles.

After deposition, the Pt particles displayed the same trend in height distribution and morphology as was discussed before for the sample shown in Fig. 4.10. Annealing in O_2 resulted in a decrease of particle density on the substrate terraces and an increase of the apparent average particle height to 0.5 nm [Fig. 4.13 (B)]. After additional annealing under the same conditions for 3 h (4 h total) the apparent average height of the Pt particles slightly increased to 0.6 nm, as can be seen in Fig. 4.14 (B).

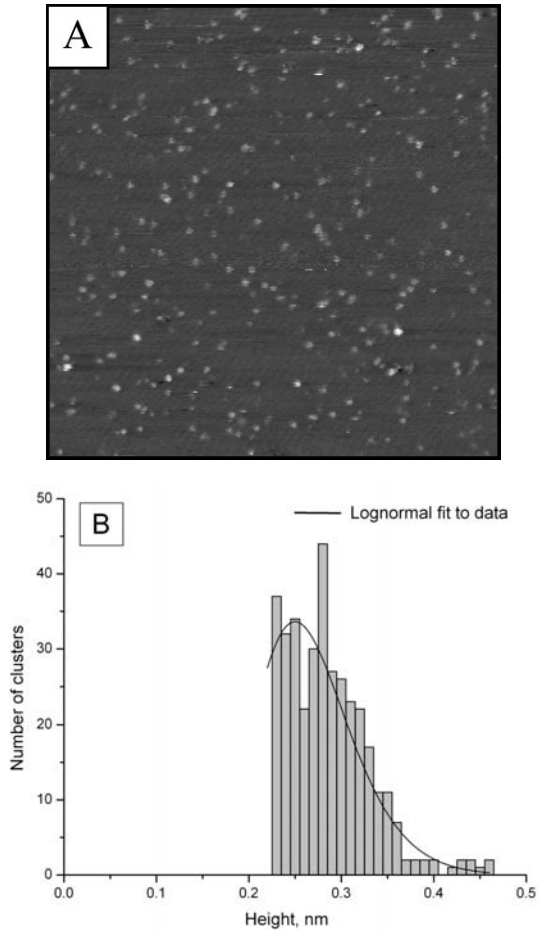

Figure 4.12: ***(A)*** *STM-image (70 × 70 nm²) of a Pt/HOPG sample with 0.2 ML Pt.* ***(B)*** *Height distribution histogram of the Pt particles.*

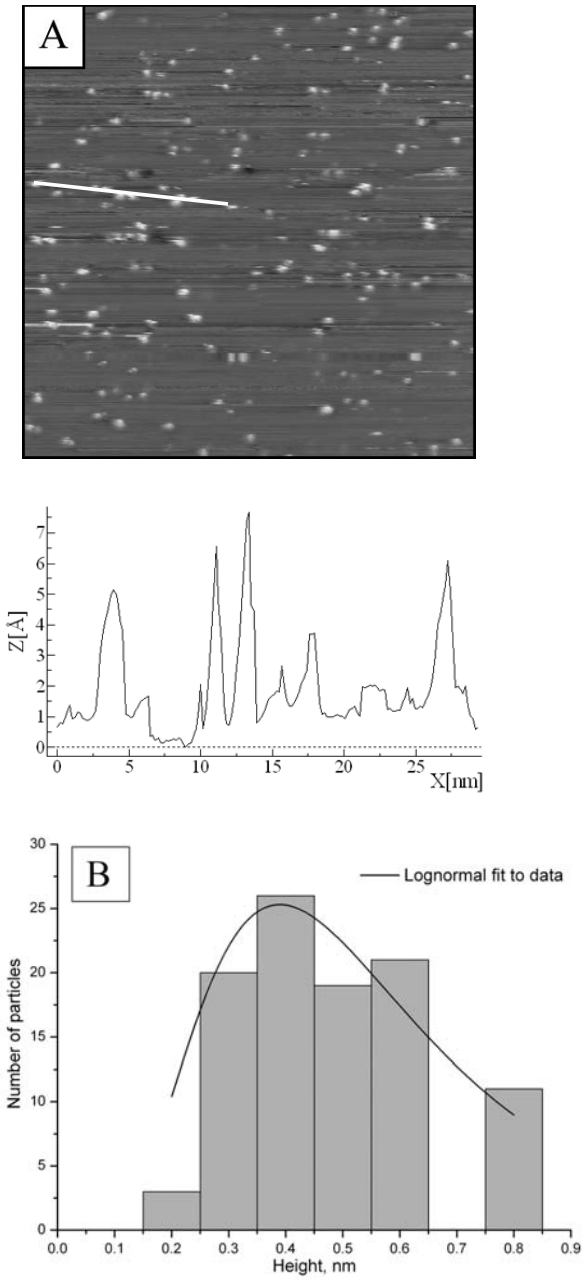

Figure 4.13: ***(A)*** *STM-image (70 × 70 nm²) of a Pt/HOPG sample with 0.2 ML Pt after annealing in O_2 for 1 h at 500°C.* ***(B)*** *Height distribution histogram of Pt particles on the same sample measured from multiple STM images taken on different sample locations. Particles within a range of heights ± 0.03 nm from the indicated values are grouped together.*

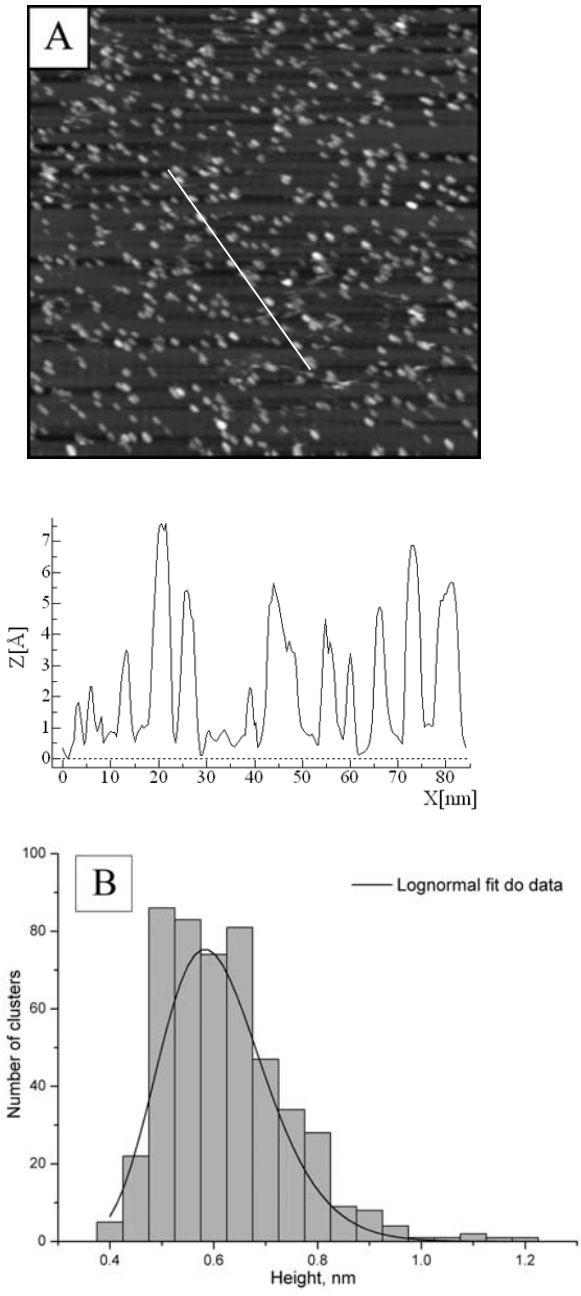

Figure 4.14: ***(A)*** *STM-image (150 × 150 nm²) of Pt/HOPG (0.2 ML Pt) after annealing in O_2 for 4 h at 500°C.* ***(B)*** *Height distribution histogram of Pt particles on the same sample measured from multiple STM images taken in different sample locations. Particles within a range of heights ± 0.03 nm from the indicated values are grouped together.*

4.3.3 Annealing in carbon monoxide

This series of the experiments was performed using Pt (0.4ML)/HOPG. The STM images after Pt deposition along with the apparent height distribution of the particles after deposition is depicted in Fig. 4.15.

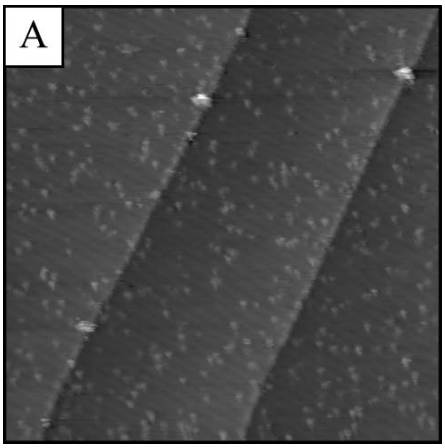

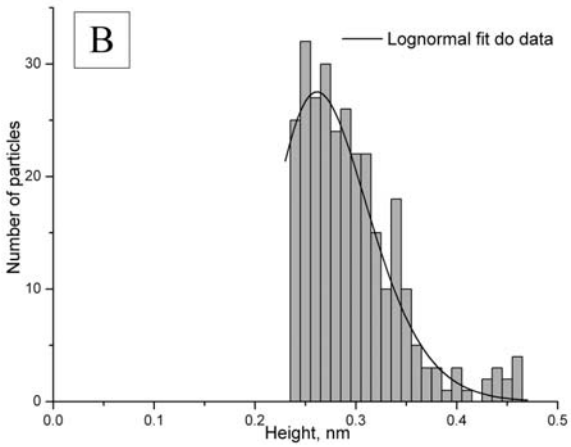

Figure 4.15: ***(A)*** *STM-image (70 × 70 nm²) of a Pt/HOPG sample after deposition of 0.4 ML Pt, showing two steps with some clusters attached to them. Two steps are one atomic layer high.* ***(B)*** *Height distribution histogram of Pt particles on the same sample deduced from STM image.*

After deposition the Pt particles show the same trend in morphology and height distribution as was discussed before. Annealing of this sample in CO (500 °C for 1 h) resulted in the appearance of larger particles as seen in the STM image [Fig. 4.16 (A)] with an apparent average height ~ 0.8 nm. Further annealing of the sample for 2 h (3 h in total) resulted in particles that appear more round [Fig. 4.17 (A)] and with a slightly smaller apparent average height of about 0.7 nm [Fig. 4.17 (B)]. Major changes in particle size/shape were observed after an additional heat treatment for 4 h (7 h total). In the STM image shown in Fig. 4.18, the Pt particles

link with neighboring particles to agglomerates consisting of several round particles. An apparent average height of the agglomerates is ~ 1.4 nm. In addition, besides agglomerates of particles, many separate particles of comparable size are visible on the terraces. Strong decoration of steps with Pt particles with an apparent height in the range of 0.4-1.2 nm has also been observed on many locations of the sample.

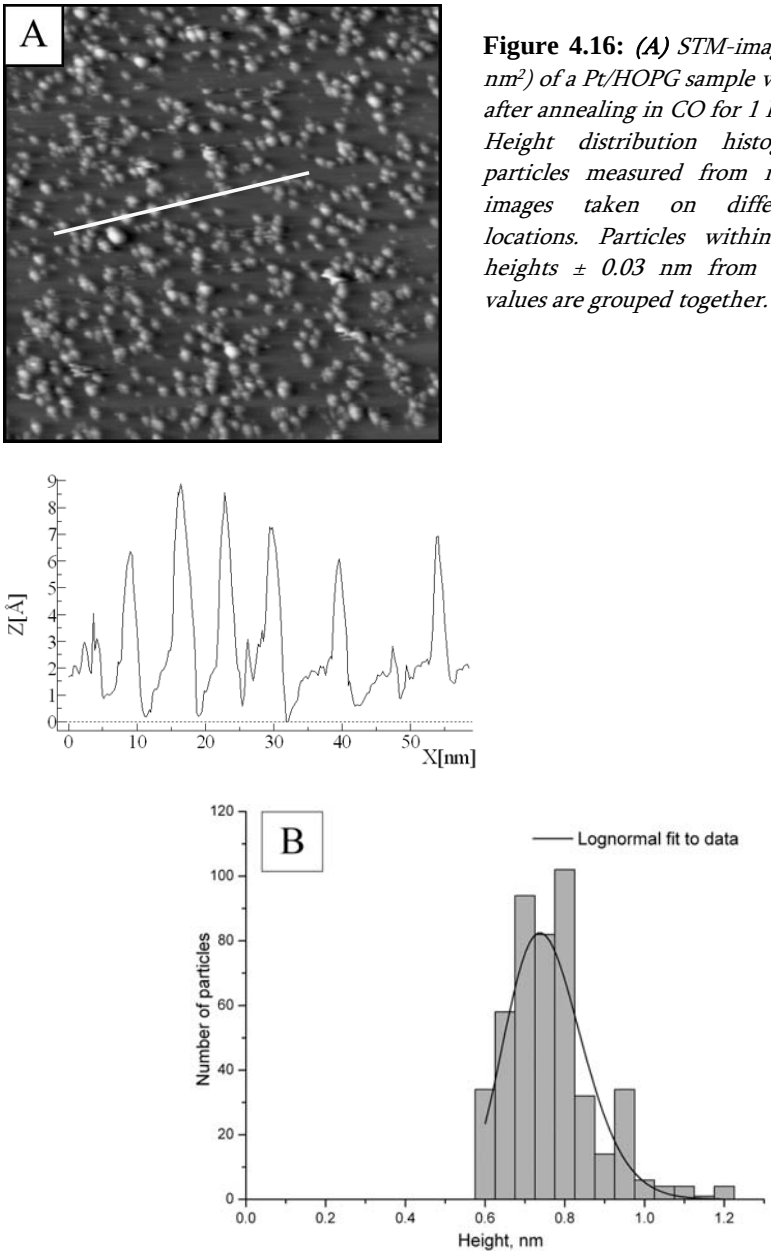

Figure 4.16: *(A) STM-image (100 × 100 nm²) of a Pt/HOPG sample with 0.4 ML Pt after annealing in CO for 1 h at 500°C.* ***(B)*** *Height distribution histogram of Pt particles measured from multiple STM images taken on different sample locations. Particles within a range of heights ± 0.03 nm from the indicated values are grouped together.*

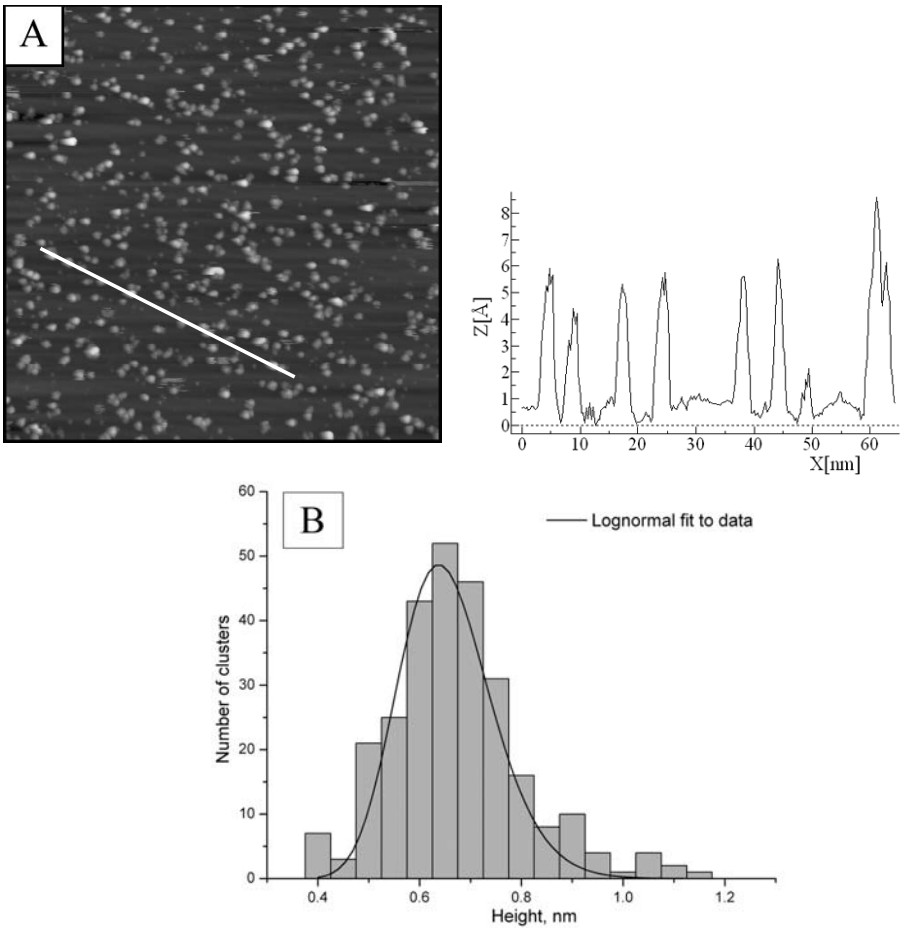

Figure 4.17: ***(A)*** *STM-image (100 × 100 nm²) of a Pt/HOPG sample with 0.4 ML Pt after annealing in CO for 3 h at 500°C.* ***(B)*** *Height distribution histogram of Pt particles measured from multiple STM images taken in different sample locations. Particles within a range of heights ± 0.03 nm from the indicated values are grouped together.*

4.3.4 Annealing in hydrogen

In the next set of experiments we started with a Pt/HOPG sample with 0.2 ML of Pt. The initial distribution of the Pt particles on this sample was similar to those of the earlier prepared Pt/HOPG samples described above. Figure 4.19 shows the STM image and height distribution histogram after annealing the sample in an H_2 atmosphere at 500 °C for 1 h. As a result of the treatment, the apparent particle mean height has increased to 0.4-0.6 nm. Compared to the annealing experiment in UHV, much larger clusters were observed on the surface and along the steps

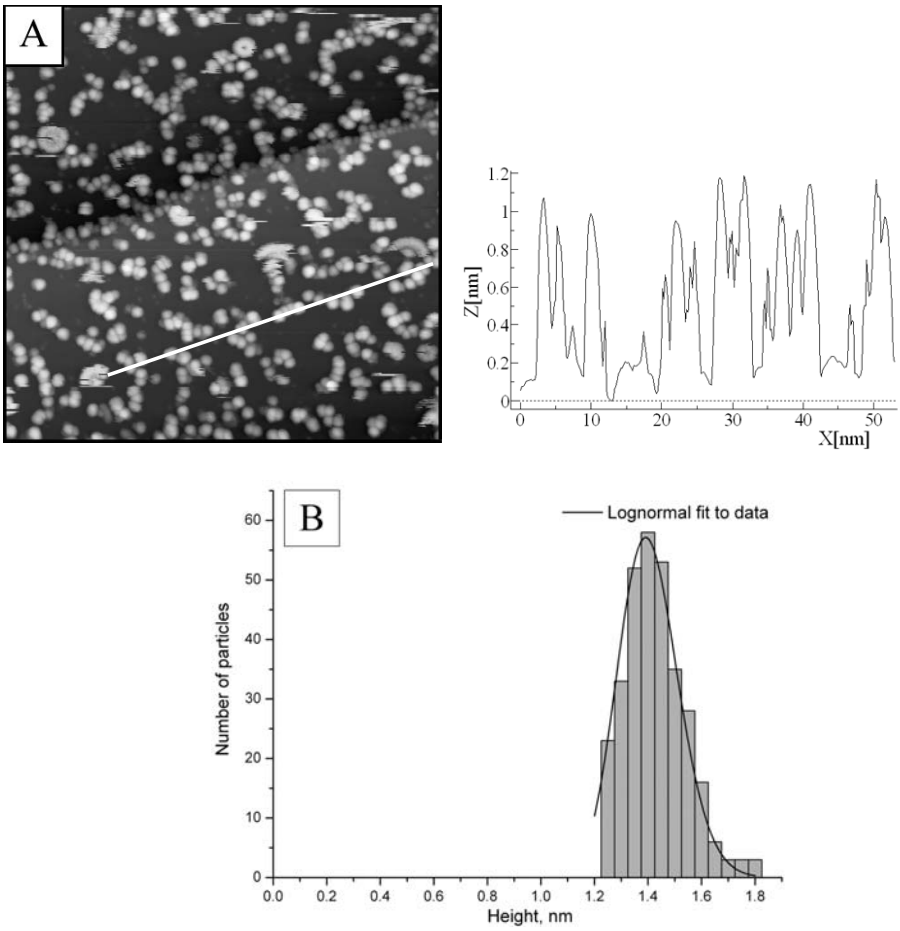

Figure 4.18: ***(A)*** *STM- image (70 × 70 nm²) of a Pt/HOPG sample with 0.4 ML Pt after annealing in CO for 7 h at 500°C.* ***(B)*** *Height distribution histogram of Pt particles measured from multiple STM images taken in different sample locations. Particles within a range of diameters ± 0.03 nm from the indicated values are grouped together.*

of the substrate. Annealing this sample for 9 h at 500 °C and $p(H_2) = 2\times10^{-5}$ mbar led to the formation of clusters with an apparent average height of 0.6-0.8 nm [Fig. 4.20 (B)]. An interesting fact is that after the last annealing in H_2 many small clusters with a height of ~ 0.2-0.3 nm coexist on the surface with much broader and higher clusters. Since many STM pictures of this series of experiments were noisy it was not possible to count exactly the number of smaller particles. Hence, they were not included in the presented histograms. At the same time larger particles exhibited two maxima in the size distribution histogram, as seen in Fig. 20 (B) with heights of ~ 0.6 nm and 0.8 nm, respectively. Interestingly, Yeung and

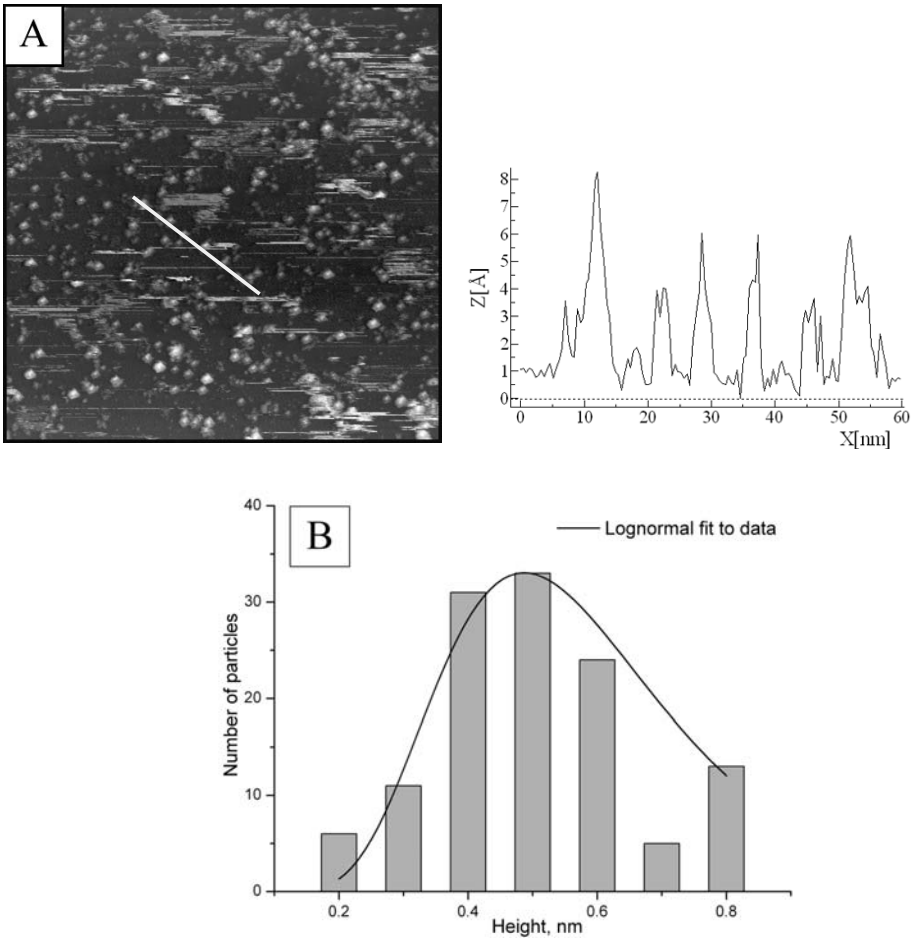

Figure 4.19: ***(A)*** *STM- image (150 × 150 nm²) of a Pt/HOPG sample with 0.2 ML Pt after annealing in H_2 for1 h at 500°C.* ***(B)*** *Height distribution histogram of Pt particles measured from multiple STM images taken in different sample locations. Particles within a range of heights ± 0.03 nm from the indicated values are grouped together.*

Wolf [14] also observed fragmentation of Pt crystallites into small irregularly shaped particles after treatment of the Pt/HOPG sample in hydrogen, however, at much higher temperature and hydrogen pressure.

In Fig. 4.21 and Table 4.1 a comparison is presented of the apparent average heights of Pt particles on a HOPG surface after various heat treatments under different conditions. It is seen that sintering occurs under all conditions studied, but it proceeds faster in a gaseous environment than in UHV.

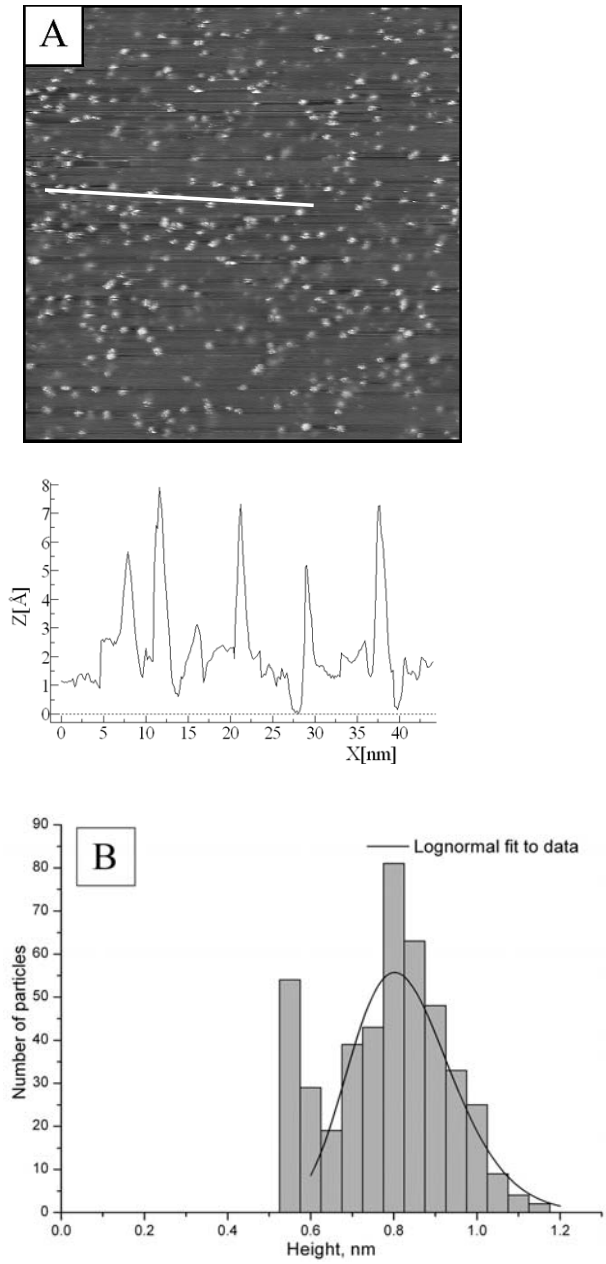

Figure 4.20: ***(A)*** *STM-image (70 × 70 nm²) of a Pt/HOPG sample with 0.2 ML Pt after annealing in H_2 for 9 h at 500°C.* ***(B)*** *Height distribution histogram of Pt particles measured from multiple STM images taken in different sample locations. Particles within a range of heights ± 0.03 nm from the indicated values are grouped together.*

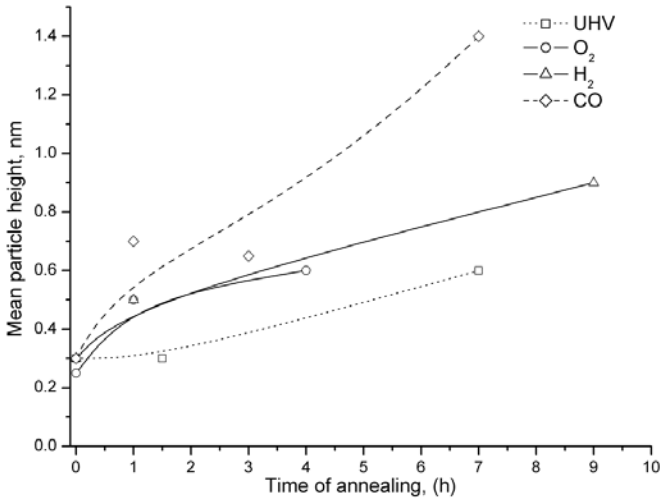

Figure 4. 21: *Plot of the apparent average platinum particle height as a function of annealing time under different conditions [Annealing temperature of 500 °C. Partial pressure of O_2, H_2 or CO (2×10^{-5} mbar)].*

Table 4.1: *Apparent mean height of Pt particles on HOPG observed after different treatments at 500 °C. The partial pressure of a gas during annealing was kept at 2×10^{-5} mbar. Annealing in UHV at 3×10^{-9} mbar.*

Gas/environ-ment used	Annealing time, (h)	Coverage, Pt (ML)	Average particle height, (nm)
UHV	0	0.3	0.3
	1.5		0.2-0.3 (small amount of 0.5-1.2)
	7		0.6
O_2	0	0.2	0.25
	1		0.4 - 0.5
	4		0.5 - 0.6
H_2	0	0.2	0.2 - 0.3
	1		0.5
	9		0.8-0.9
CO	0	0.4	0.3
	1		0.7-0.8
	3		0.65
	7		1.4

4.4 Discussion

Due to differences in the surface energy between HOPG (0.07 J/m^2) [122] and platinum (2.30 J/m^2) for Pt(111) [123] and the lattice mismatch, platinum deposits on HOPG are expected to grow according to the Volmer-Weber mode, which implies that the forces between the metal atoms are dominating (see § 3.1). This means that during Pt deposition three-dimensional metal clusters promptly form even when the total amount of deposited metal is less than one atomic layer. In the present study upon deposition irregularly shaped 2-D/3-D platinum particles and randomly distributed over the substrate were registered. The apparent average height of the particles was about 0.3 nm. This implies that the growth mode in the range of Pt coverages used in the study may indeed follows the VW growth mode that is also in accordance with MD simulations [124, 125]. This also testifies that the "up-step" diffusion barrier for Pt on Pt is low enough to overcome at room temperature. The propensity of Pt to decorate the step edges just after deposition was not very much manifested and only a small fraction of the particles was registered there. Probably, just after the start of deposition the steps are not sufficiently effective as sinks, and the aggregates on atomically smooth surface areas are viable in the competition for the building material. But nevertheless these results indicate that the diffusion barrier for the individual Pt atom on the flat HOPG surface is low enough to allow the atoms to be mobile. Platinum particles of a similar morphology were also imaged by using STM in [16]. However, in contrast to this work we have not detected single Pt atoms, Pt dimers and Pt trimers on the HOPG samples.

The quantized height of Pt particles found at step edges in our study suggests the idea that here probably "magic number" clusters are observed. This assumption is based on the following considerations. Using the model described in § 3.3, the hard-sphere radius of a free-standing n-atom cluster can be calculated. Assuming a hemispherical shape of a cluster its height above the support equals its radius. Then the radii of several Pt "magic number" clusters are as follows: Pt_{13} (3.6 Å), Pt_{55} (5.8 Å), Pt_{147} (8.1 Å), Pt_{309} (10.3 Å), Pt_{561} (12.6 Å), and for the minimal 3-D cluster Pt_4 (2.4 Å). As one can see the cluster's radius increases stepwise of 2.2-2.3 Å going from 13 to 561 "magic number" cluster. Though the height difference between the Pt clusters at the HOPG step edges are found to be smaller (about 1 Å) (see Fig. 4.7 and Fig. 4.8), from those calculated for free "magic clusters", these results as well can reflect the possibility of the formation of "magic clusters". This assertion is based on the fact that the support can influence the arrangements of atoms within "magic clusters" and their electronic and structural properties are expected to change in comparison with equivalent free clusters. For example, by total energy calculations for Ag clusters supported on a Ag(001) substrate [126] it

has been shown that the relative stability of supported clusters is governed by the underlying geometry of the substrate leading to completely different "magic numbers" in 2-D systems. Tetramer and hexagonal heptamer are the first two "magic numbers" in such systems. For instance, the formation of stable Pt clusters (heptamers) was suggested by Rosenfeld *et al.* [127] on Pt(111) surface at coverages below 0.1 ML at temperatures above 500 K, which appeared to be stable with respect both decomposition and to further growth. Recently performed MD simulations [128] also established the existence of well-defined "magic numbers", different from those characteristic for free particles due to particular features of interaction at the metal/oxide interface. The formation of "magic clusters" which are stable at certain sizes on a particular surface is reviewed in [129]. Recently it was possible to observe some of such "magic clusters" by STM [130-132].

It should be noted that the physico-chemical properties of a cluster are even more affected when it is placed near a defect site, e.g., step edges. For example, stable Ga trimers and heptamers on the GaAs(001) surface were found in [130]. The clusters might be attracted by step edges. These clusters possessing 9 and 21 electrons in molecular orbital states are close to the values (8 and 20, respectively) needed to form a closed electronic shell. Interestingly that because of its stability some of these heptamers were found to move along the missing dimer row of the surface preserving their shape. This important property of "magic number" clusters to act as a fundamental unit in mass transport phenomena was also registered in [131]. It is believed that the described behavior of the clusters can also take place in the Pt/HOPG system. At steps Pt clusters with certain discrete dimensions are more often observed than on the terraces of HOPG.

As well, due to the fact that in metal particles of a few nanometers in diameter, bulk descriptions of the electronic structure are no longer valid and progressively smaller metal particles exhibit a size-induced metal-to-insulator transition: below a certain threshold diameter they are no longer metallic [133-135]. Experimentally, non-metallic properties of Pd, Ag, Cd and Au nanoparticles of 1 nm diameter on a graphite substrate were established by Vinod *et al.* [44]. An energy gap reaching values up to 70 meV at small cluster sizes was registered in that study. Scanning tunneling spectra revealed that Pt nanoparticles supported on a TiO_2 (110) surface [136] below 20 Å in diameter exhibit nonmetallic behavior, while those above 40 Å metallic. The above findings are in line with the study of Bettac *et al.* [137] for Pt clusters on HOPG. Scanning tunneling spectroscopy in UHV at liquid helium temperatures performed in that work registered distinct peaks in the conductivity of this cluster-on-surface system. For negative voltages, the peak separations scaled with the inverse particle height. More recent studies [138] on size-selected Pt cluster ions deposited on a graphite surface also corroborate these data. Moreover, indications have been found that the electronic

structure of the clusters depends both on size and the geometric structure and/or interaction with the surface.

Apart from the effects described above, the real nanocluster dimensions can be obscured by tip effects.

Diffusion processes of a material on a support are among the primary factors influencing the structure of deposits. To the author's knowledge there is no experimental data available on the diffusion coefficient for Pt atoms or clusters on HOPG. According to MD simulations performed for Pt clusters on a graphite surface [139] at room temperature clusters with less than 40 atoms are very mobile with a two-dimensional diffusion coefficient higher than 10^{-11} m^2/s, but decreasing rapidly with size. The diffusion coefficient of larger clusters was found to be variably size-dependent with local minima for cluster sizes of 50 and 300 Pt atoms and a local maximum for a cluster size of 100 atoms. In addition, the mismatch between the bottom layer of Pt and graphite also affects the overall Pt-graphite affinity and, hence, the cluster mobility. It was found that the presence of a nearby Pt cluster can greatly affect the mobility. The aggregation of two 50-atom clusters to form a single cluster was observed with the simulation. These relatively stable new clusters resembled previous experimentally observed network of connected Pt nanoparticles on graphite. By MD simulations [140] it was also found that the average atomic diffusion coefficient for the single Pt cubic and spherical clusters at about 500 °C is 2×10^{-9} and 4×10^{-9} m^2/s, respectively. In addition, it was established that the solid-liquid transition for a 256-atom Pt cluster of cubic shape and for a ball shaped cluster of 260 Pt atoms, deposited on a graphite substrate takes place at 727 and 747 °C, respectively.

Recent quantum-mechanical calculations also show that the interaction of Pt atoms and clusters of different size with the HOPG surface is weak. For instance, according to DTF calculations performed by Okazaki-Maeda *et al.* [141] the interaction between graphene and Pt decreases in the order of a single Pt atom, a Pt cluster (Pt_{10}), and a Pt(111) monolayer. The adhesive energy between graphene and the Pt(111)-monolayer is 0.09 eV/atom. This implies very weak interaction between these structures. For a Pt atom it was found that the Pt-C bond length is 2.31 Å and the adsorption energy is 2.82 eV/adatom. The distance between graphene and the bottom layer of the Pt_{10} cluster is about 2.7 Å. These results imply stronger interaction between this cluster and graphene than the Pt-monolayer/graphene interaction. Further DFT study [142] also revealed that the interfacial interaction between Pt_n and a non-defected graphene sheet becomes weaker with the number of Pt atoms in clusters: 2.17 eV/atom for Pt_1, 0.63 eV/atom for Pt_2 and 0.15 eV/atom for triangular Pt_3. The tetrahedral Pt_4 cluster was found to interact more strongly with the support in comparison with the triangular Pt_3 cluster. The adsorption energy for a Pt atom on the vacant site of a

graphene sheet is 8 eV/adatom. This energy is stronger than the formation energy of a Pt-Pt bond (~ 2 eV/bond) for small clusters. It was also established that a Pt atom is stably adsorbed on the bridge site between two carbon atoms with adsorption energy of about 2 eV.

As registered in this study annealing in the presence of the gases results in a faster formation of larger (higher) clusters. This implies that the gaseous environment influences the growth process. The thermodynamic contribution of the gas phase can be included in the energetic through the chemical potential:

$$\mu = (\partial G^g / \partial n)_{p,T} = \mu^0 + RT \ln(p / p^0),$$

where G^g is the Gibbs free energy of the gas, n the number of the moles of gas, μ^0 a reference potential, R the gas constant, T the temperature, p the pressure and p^0 the standard state pressure. When the pressure is increased over 5 orders of magnitude from 10^{-10} mbar to 10^{-5} mbar the chemical potential is increased by an amount of $5RT$=12 kJ/mol or ~ 0.12 eV per at room temperature and 31 kJ/mol or ~ 0.32 eV at 500 °C per gas molecule. Thus, the chemical potential of the gas phase can appreciably contribute to the surface free energy γ of the surface layer (deposited phase), which for a given temperature T and pressure p is given by:

$$\gamma(T, p) = [G^s(T, \{N_i\}) - \sum_i N_i \mu_i(T, p)] / A,$$

where G^s is the Gibbs free energy of the surface, and N_i is the number of adsorbed molecules of species *i*. In addition, impinging molecules from the gas phase modify continuously the local energy balance in the system. Also, as was mentioned in § 4.2.2 the adsorption of, e.g., oxygen induces structural distortion in the clusters. This property has been coined "structural dynamical fluctionality" and it is unique to clusters in the nanometer size range [143]. In view of the weak interaction between Pt clusters and a HOPG surface, discussed above, it may be supposed that the redistribution of charge upon gas adsorption will influence cluster mobilities on the support and thus the growth processes. The same processes may lead also to the weakening of the bond between the atom interacting with an adsorbate and neighboring atoms. In the following some assumptions regarding these issues are discussed.

In earlier work by Shi and Masel [144] for Pt particles in a H_2 atmosphere, it was calculated that at 900 K the hydrogen coverage on all of the facets of Pt particles should be negligible at pressures below 5×10^{-4} Torr. But at higher pressures various facets are filled with hydrogen, first the (100) and last the (111) facets. Also on the experimental side, e.g., by hydrogen TPD studies [145] from Pt clusters (consisted on average of 6-12 atoms) supported on a series of zeolites, SiO_2 and γ-Al_2O_3, reversible desorption of chemisorbed hydrogen at about 175 °C has been registered. Besides chemisorbed hydrogen, at least three peaks at *ca*. 250, 400 and 600 °C, irreversibly desorbed hydrogen, were observed and assigned to

spillover hydrogen. These data point out that under the annealing conditions applied in this study almost no hydrogen should be adsorbed on the Pt particles. In this case mainly temperature governs the clusters and then the transport of the material on the HOPG surface apparently can occur by means of the movement of individual Pt clusters, i.e. coalescence. This mechanism of the cluster growth seems to be preferred because the enthalpy of vaporization of Pt ($\Delta H^0_{f,\ 298.15}$) is about 565 kJ/mol [146] and its vapor pressure at 527 °C is 9.77×10^{-30} bar [147] and the energy required to transfer Pt atoms from a particle to the substrate is about 527 kJ/mol [146]. This implies that intercluster transport by free Pt atoms will be very low at the temperatures used in the present study (500 °C). At the same time the cohesive energy is found proportional to the cluster size to the -1/3 power. Thus, for small Pt clusters it is considerably lower than that of bulk Pt, for example, for the cluster with 10 atoms it is *ca*. 337 kJ/mol [148]. Hence, probably if tiny clusters initially are available in the system, Ostwald ripening may take place. However, it should be noted that the samples were cooled in the presence of H_2, CO or O_2 and under these conditions H, CO or O may adsorb on platinum. In addition as it was noted in § 4.2.2, very small clusters have different adsorption characteristics than larger ones. On the basis of the recent DFT studies [109] one can assume that sub-nanometer Pt clusters consisting of up to 10 Pt atoms can dissociatively adsorb a rather large quantity of hydrogen. This in turn may have a significant impact on their interaction with the HOPG surface. Also, during heating and cooling in a H_2 atmosphere, the surface is covered by hydrogen and this may affect the surface/cluster chemistry/physics. This can result in an increase of the mobility of the Pt clusters on the surface and they may grow due to coalescence.

After annealing the Pt (0.2 ML)/HOPG sample in H_2 for 1 h, a rather narrow size distribution of Pt particles centered at 0.5 nm is observed (Fig. 4.19). Curiously, after much longer annealing time (9 h), as seen in Fig. 4.20 there are two peaks centered at about 0.5 and 0.8 nm. This may indicate a bimodal distribution of the Pt particle size. A bimodal size distribution of clusters was registered by Lai *et al.* [149] for the $Ag/TiO_2(110)$ system after exposure to 10 Torr O_2 at ambient temperature. This was attributed to Ostwald ripening, since there were two distinct average Ag cluster sizes. Hence, the Pt particle size distribution after annealing in H_2 found in this study may also indicate that cluster growth under H_2 atmosphere takes place via Ostwald ripening. However, at present the shortage of available data does not allow to make a statistically unambiguous assertion regarding this issue. As was noted above, after longer annealing in H_2, much smaller particles were registered in addition to large particles. This again may point to Ostwald ripening or to redispersion of Pt clusters in the presence of H_2. A more detailed study is necessary to clarify the origin of this phenomenon.

The Pt (0.3 ML)/HOPG sample after annealing in UHV for 7 h (Fig. 4.11) showed a narrow size distribution of Pt particles centered at 0.6 nm, with a minor amount of larger clusters (0.8-1.3 nm). The same trend in size distribution is observed after heating the Pt (0.2 ML)/HOPG sample in O_2 for 4 h at 500 °C, as seen in Fig. 4.14. After annealing the Pt (0.4 ML)/HOPG sample in CO the size distribution of the Pt particles on this sample becomes more symmetric, but a small amount of higher particles is present in all histograms (Fig. 4.16 - Fig. 4.17). The average height of the Pt particles increases with time in both CO and O_2 atmospheres.

According to [144], the CO coverage on all the facets of Pt particles in a carbon monoxide atmosphere should be negligible at 900 K at pressures below 1×10^{-5} Torr. In view of these data the amount of adsorbed CO on the surface of Pt particles is very small under the experimental conditions used in the present study. But as noted in § 4.2.2, the chemistry of CO adsorption and desorption is size-dependent and on tiny Pt clusters CO may adsorb more strongly than on large ones. For example, Altman and Gorte [150] have found that CO desorbs from supported Pt particles (1.1 nm) on Al_2O_3 in a single peak at 510 K. For larger particles, there was the second desorption peak at 400 K. Again, similar as for H_2 during heating and cooling in a CO atmosphere, the surface is covered by CO and this may affect the surface/cluster chemistry/physics. It is worth noting that in an atmosphere of CO under certain conditions Pt nanoparticles can undergo CO-assisted Ostwald ripening in which the mass transport proceeds via surface carbonyl intermediates. To this possibility pointed out Berkó *et al.* [151] in the study of Pt/TiO_2(110)-(1×n) system under 10^{-3}-10 mbar of CO by STM. It was detected that CO adsorption induced a significant increase in the initial size of the Pt particles and led to the disruption of the smaller Pt clusters at lower CO pressures. Indication of the disruption of Pt crystallites was also observed by Raskó [90], who studied CO adsorption (0.01-10 Torr, 300 K) on supported Pt catalysts with diffuse reflectance infrared spectroscopy.

Similar to CO, theoretical calculations already mentioned in § 4.2.2 [103] predict a significant increase of the strength of oxygen interaction with tiny Pt clusters. In turn, the experimental studies also registered this phenomenon [152-154]. Putna *et al.* [152] by TPD have found that O_2 desorbs from Pt particles (8.3 nm) supported on α-Al_2O_3(0001) in the peak centered at 800 K, whereas from smaller particles (2 nm) the desorption peak was centered at about 950 K, despite a much higher saturation oxygen coverage on these particles. As well, TPD studies [154] revealed oxygen desorption peaks at 645, 719 and 755 K from the Pt (1 wt. %)/SiO_2 system (Pt dispersion of 97 %). This may suggest that at least a small part of Pt clusters may be oxidized under the conditions applied in the present study. According to phase diagram for bulk platinum oxides calculated recently by

Seriani [155] employing DFT, α-PtO_2 is the thermodynamically stable bulk phase at low temperatures and low oxygen pressures. Bulk Pt_3O_4 is found to be thermodynamically stable in a region between 870 K and 974 K at atmospheric pressure. PtO exists only as a metastable phase. Considering the oxidation of Pt clusters the author found that as the diameter of the cluster diminishes, the region of stability of α-PtO_2 expands to higher temperatures. For clusters smaller than 5 nm, the Pt_3O_4 phase is stable only at temperatures higher than about 1050 K. Interesting fact is that similar to HOPG in α-PtO_2 layers are held together only by weak van der Waals forces in the (0001) direction [155]. The surface free energy of α-PtO_2(0001) is only 2 meV/Å^2, so that an α-PtO_2 cluster is expected to be composed of an isolated O-Pt-O trilayer. Based on these findings as well as on early work by Wynblatt [156] and more recent by Rickard *et al.* [157], I assume that the growth of Pt particles in Pt/HOPG system could occur due to intercluster transport of α-PtO_2. Therefore, the process of Ostwald ripening may become possible. In addition, during heating and cooling in an O_2 atmosphere, the surface may adsorb oxygen and this may affect the surface/cluster chemistry/physics.

It has been suggested that the evolution of the particle shape distribution can give insight into the mechanism of the particle growth [158, 159]. For instance, the size distribution has been shown to tail toward large sizes if coalescence of particles takes place [159, 160]. In the study of the scaling solution to a cluster coalescence model [161], which adopted the mean field approximation used by Smoluchowski [162] and considered the case when mass transport in the system proceeds by faster diffusion of the atoms on the terraces compared with the exchange of atoms between clusters and nearby terraces, it was established the scaled island size distributions are right-skewed and the scaling function is not sensitive to the initial cluster size distribution. In addition, it was found that the most probable cluster size as well as the width of the distribution increase with time. Instead, the kinetics of Ostwald ripening results in a stationary (self-similar) particle size distribution which exhibits an almost symmetric shape, but tails to small sizes (smaller particles are continually generated as sintering proceeds) [161, 163]. The inverse power-order in mean particle diameter increases linearly with time according to this growth law. This model also predicts that there should be a cut off in the size distribution at a diameter < twice the mean diameter [163]. Taking into account these notions, the registered shape of the histograms after annealing the Pt/HOPG samples in UHV, O_2 and CO indicate that the Pt particles may grow here due to coalescence of smaller Pt particles. Also clear upper bound (2 times the mean diameter) on the particle sizes in the annealed samples as predicted by Ostwald ripening mechanism was not observed in this study. At the same time a shortage of the experimental data does not allow making a definitive conclusion about the particles growth mechanism. The tip-induced relocation of

the clusters observed in some cases in the present work as well as by other workers demonstrates that the interaction of Pt with HOPG is weak and, thus, the coalescence mechanism of sintering should dominate in this system. This is further supported by the observed morphology of the cluster agglomerates. Some clusters have been observed with a clear boundary in-between, indicating that entire Pt particles moved till collision with other particles. Such cluster morphology is not expected for systems where particle growth proceeds through Ostwald ripening. This particular Pt cluster behavior is observed following annealing the Pt/HOPG samples in CO for a longer time. In this context it is worth mentioning that Ag and Au clusters [33] were found to be weakly bound to and incommensurate with the HOPG substrate and according to the study by Ganz *et al.* [4] Ag clusters can diffuse over the surface at room temperature and coalesce forming small stable groups. However, it cannot be excluded that in the Pt/HOPG system, Ostwald ripening can also occur to some extend. As noted in [159] the absence of small particles in the system, and a skew to the large sizes in the particle distribution histogram does not immediately imply that Ostwald ripening does not take place, since it is possible that due to very high mobility small clusters disappear more quickly than they can be registered. In addition, according to new sintering mechanism models [164, 165] coalescence as well as Ostwald ripening processes can be described by size right-skewed distributions. Thus, at present the issue of a relationship between particles size distributions and sintering mechanisms is under debate. Taking into account all the above works one can assert that the details of the growth of Pt particles on a HOPG surface deserve further studies.

In connection with the mechanisms of Pt particles sintering I would like to mention very interesting results obtained by MD simulations revealing a novel surface diffusion phenomenon for large Au clusters on a graphite surface [166]. The authors predicted that large (hundreds of atoms) 3-D gold clusters adsorbed on graphite may undergo an anomalous diffusive motion with surprisingly high rates, occurring through a collective slip-diffusion mechanism, i.e. the alternation between local oscillatory "sticking" states and free diffusive motion, involving sliding trajectories. For a Au_{140} cluster with *fcc* structure and a truncated-octahedral morphology adsorbed on the basal plane of graphite the significant slip could be initiated at about 500 K. Below this temperature the clusters display some slip but less frequently. It was suggested that the high mobility of the cluster on the surface originates from its interfacial incommensurability and on the coupling strength between the adsorbate and the surface. Extending the research further the diffusion characteristics of gold clusters (consisting of 38, 79, 140, or 586 atoms) on graphite was studied near a one-layer high step edge [167]. It was found that at low temperatures the cluster is trapped to a region of the lower terrace

diffusing along the step edge. At higher temperature it may escape from the step-edge region and diffuse on various regions of the bottom terrace. As the temperature increases, the escape probability increases. For the larger clusters, higher temperatures are required to obtain comparable escape probabilities.

Besides the growth modes and sintering mechanisms, the shape and structure of supported metal particles is a quite important issue for understanding of supported metal catalysts. It is well-known that the morphology of small metal particles can change in the presence of a gas atmosphere [146, 168, 169]. In an early study by Lee *et al.* [168] it was found that clean micrometer-sized Pt particles (>1 μm) have a spherical shape with distinct (100) and (111) facets upon long annealing (24 h and more) at 1200 °C in 10^{-7} Torr oxygen. The particles did not show a cubo-octahedral shape with sharp edges as predicted by the Wulff construction. Instead, carbon contaminated Pt particles had a cubo-octahedral shape with large (111), (100) and (110) facets and curved boundaries. Calculations concerning the influence of H_2 and CO on the ECS of supported Pt particles [144] suggest that the coverage of 10 % of a monolayer may affect the particle shape. The equilibrium shape of the particles was not affected by nitrogen, which does not adsorb on platinum.

In our study platinum particles were of a much smaller size than in the above mentioned work and atomic resolution of the particles surface was not achieved. Tip convolution effects make it difficult to determine the precise 3-D morphology of the particles and it was only possible to observe some changes in their global shape. For instance, after annealing in oxygen for 4 h (Fig. 4.13) the Pt particles appear to be elongated. After annealing in CO for 1 h the shape of the particles was more spherical (see Fig. 4.15) and longer annealing produced round particles distributed over the terraces and along the step edges (see Fig. 4.17). The presence of H_2 during annealing also resulted in the formation of larger particles of globular shape. Larger particles annealed in UHV were of similar shape. The smaller particles, however, showed an irregular perimeter.

In conclusion it is worth noting, that numerous studies dealt with the morphology of platinum deposits on a HOPG surface prepared by a wide range of methods. However, the behavior of platinum deposits on a HOPG surface in a mixture of gases - an issue of paramount importance to catalysis, attracted much less attention. In this context it is suggested to investigate in detail the influence of reaction mixtures of different gases, for instance $CO+O_2$, on the morphology of Pt particles. Such studies can give insight into the interplay between particular size, structure of Pt particles and their catalytic performance. The first theoretical as well as experimental studies in this direction are already available and are very promising [170-173].

4.5 Conclusions

The results of Pt vapor deposition on the HOPG(0001) surface and subsequent annealing in UHV, O_2, CO and H_2 are summarized as follows:

1. Platinum deposited on the HOPG(0001) surface in the coverage range of 0.2-0.4 ML initially forms randomly distributed and irregularly shaped 2-D/3-D particles with an average height of 0.2-0.3 nm. A small part of the particles decorates the step edges of the substrate. Annealing the Pt (0.3 ML)/HOPG system in UHV (7 h total) results in the formation of a very narrow Pt particle size distribution centered at 0.5-0.6 nm.

2. After annealing in oxygen, $p(O_2)=2\times10^{-5}$ mbar for 1 h at 500 °C, the average height of the particles for 0.2 ML Pt increased to 0.5 nm and after additional annealing for 3 h to 0.6 nm.

3. After annealing the Pt(0.4 ML)/HOPG sample in the presence of CO, $p(CO)=2\times10^{-5}$ mbar at 500 °C for 1 h, the apparent average particle height of 0.7-0.9 nm was observed. After annealing for an additional 6 h under identical conditions, the average size of the particles increased to 1.3-1.5 nm. Particles of a globular morphology were found to assemble into aggregates consisting of several separate particles. Very strong decoration of step edges with spherical particles was found.

4. After annealing the sample with 0.2 ML of Pt in H_2, $p(H_2)= 2\times10^{-5}$ mbar at 500 °C for 1 h the apparent average particle height was centered at *ca.* 0.5 nm. Prolonged annealing for 9 h (total) resulted in an increase of the average particle height to 0.8 nm. The histograms of particles height distributions exhibited two peaks in the range of *ca.* 0.5-1.0 nm. In addition to these particles, smaller particles with an apparent height of 0.2-0.3 nm have been registered.

5. The annealing experiments in UHV and gaseous environment (O_2, CO and H_2) indicate that in all the cases the growth of Pt nanoparticles may occur by coalescence.

4.6 References

[1] A. F. Wells, *Structural Inorganic Chemistry,* 5th ed., (Oxford University Press, Oxford, UK, 1984).
[2] W. F. Egelhoff, Jr. G. G. Tibbetts, Phys. Rev. B **19** (10), 5028-5037 (1979).
[3] V. A. Self, P. A. Sermon, J. Phys.: Condens. Matter **1**, SB221-SB224 (1989).
[4] E. Ganz, K. Sattler, J. Clarke, Surf. Sci. **219** (1-2), 33-67 (1989).
[5] S. Eppell, G. S. Chottiner, D. A. Scherson, G. Pruett, Langmuir **66**, 1316-1319 (1990).
[6] A. Humbert, M. Dayez, S. Granjeaud, P. Ricci, C. Chapon, C. R. Henry, J. Vac. Sci. Technol. B **99** (2), 804-805 (1991).
[7] U. Müller, K Sattler, J. Xhie, N. Venkateswaran, G. Raina, J. Vac. Sci. Technol. B **99** (2), 829-832 (1991).
[8] S. J. Eppell, Ph. D. Thesis, Case Western Reserve University, USA (1991).
[9] K. L. Yeung, E. E. Wolf, Vac. Sci. Technol. B **99** (2), 798-803 (1991).
[10] J. Shen, Ch. Zhu, Z. Ma, S. Pang, Appl. Surf. Sci. **60/61**, 648-652 (1992).
[11] Z. Ma, Ch. Zhu, J. Shen, S. Pan, Vacuum **43** (11), 1115-1117 (1992).
[12] S. Lee, H. Permana, K. Y. S. Ng, J. Vac. Sci. Technol. B **10** (2), 561-565(1992).
[13] K. L. Yeung, E. E. Wolf, Catal. Lett. **12**, 213-226 (1992).
[14] K. L. Yeung, E. E. Wolf, J. Vac. Sci. Technol. A **10** (4), 651-656 (1992).
[15] K. L. Yeung, E. E. Wolf, J. Catal. **143** (2), 409-429 (1993).
[16] G. W. Clark, L. L. Kesmodel, J. Vac. Sci. Technol. B **11** (2), 131-136 (1993).
[17] J. Valenzuela, L. Morales de la Garza, M. Avalos-Borja, S. Fuentes, J. Phys. Cond. Matt. **55** (33A), A413-A416 (1993).
[18] Y. Murakami, K. Naoi, K. Yahikozawa, Y. Takasu, J. Electrochem. Soc. **141** (9), 2511-2513 (1994).
[19] K. Sattler, G. Raina, M. Ge, J. Xhie, N. Venkateswaran, D. Siegel, J. Appl. Phys. **76** (l), 546-551 (1994).
[20] H. Permana, S. Lee, K. Y. S. Ng, Catal. Lett. **24**, 363-376 (1994).
[21] S. Lee, H. Permana, K. Y. S. Ng, Carbon **32** (1), 145-153 (1994).
[22] S. Lee, H. Permana, K. Y. S. Ng, Catal. Lett. **23**, 281-292 (1994).
[23] H. Xu, H. Permana, Y. Lu, K. Y. S. Ng, Surf. Sci. **325** (3), 285-293 (1995).
[24] H. Xu, K. Y. S. Ng, J. Vac. Sci. Technol. B **13** (6), 2160-2165 (1995).
[25] C. Binns, S. H. Baker, A. M. Keen, S. N. Mozley, C. Norris, H. S. Derbyshire and S. C. Bayliss, Phys. Rev. B **53** (11), 7451-7459 (1995).
[26] Z. Rakocevic, S. Strbac, N. Bibic, D. Perusko and T. Nenadovic. Thin Solid Films **257** (1), 83-87 (1995).
[27] K. L. Yeung, K. H. Lee, E. E. Wolf, J. Catal. **156** (1), 120-131 (1995).
[28] A. Bifone, L. Casalis, R. Riva, Phys. Rev. B **51** (16), 11043-11048 (1995).
[29] G. M. Francis, L. Kuipers, J. R. A. Cleaver, R. E. Palmer, J. Appl. Phys. **79** (6) 2942- 2947 (1996).

[30] L. Bardotti, P. Jensen, A. Hoareau, M. Treilleux, B. Cabaud, Surf. Sci. **367** (3), 276-292 (1996).
[31] A. Wawro, R. Czajka, A. Kasuya, Y. Nishina, Surf. Sci. **365** (2), 503-510 (1996).
[32] I. M. Goldby, L. Kuipers, B. von Issendorff, R. E. Palmer, Appl. Phys. Lett. **69**, 2819-2821 (1996).
[33] G. M. Francis, I. M. Goldby, L. Kuipers, B. Von Isseldorff and R. E. Palmer, J. Chem. Soc.-Dalton Trans. **55**, 665-671 (1996).
[34] H. Xu, K. Y. S. Ng, J. Vac. Sci. Technol. B **15** (2), 186-191(1997).
[35] H. Hövel, Th. Becker, A. Bettac, B. Reihl, M. Tschudy, and E. J. Williams, J. Appl. Phys. **81** (1), 154-158 (1997).
[36] P. J. Durston, J. Schmidt, R. E. Palmer, J. P. Wilcoxon, Appl. Phys. Lett. **71** (20), 2940-2942 (1997).
[37] C. M. Whelan, C. J. Barnes, Appl. Surf. Sci. **119**, 288-300 (1997).
[38] Z. H. Zhang, P. Kulatunga, H. E. Elsayedali, Phys. Rev. B **56** (7), 4141-4148 (1997).
[39] P. Marcus, C. Hinnen, Surf. Sci. **392** (1-3), 134-142 (1997).
[40] S. J. Carroll, S.G. Hall, R. E. Palmer, R. Smith, Phys. Rev. Lett. **81** (17), 3715-3718 (1997).
[41] S. J. Carroll, P. D. Nellist, R. E. Palmer, S. Hobday, R. Smith, Phys. Rev. Lett. **84** (12), 2654-2657 (2000).
[42] A. Howells, T. Harris, K. Sashikata, G. S. Chottiner, D. A. Scherson, Solid St. Ionics **94**, 115-121 (1997).
[43] I. Lee, K.-Y. Chan, D. L. Phillips, Appl. Surf. Sci. **136** (4), 321-330 (1998).
[44] C. P. Vinod, G. U. Kulkarni, C. N. R. Rao, Chem. Phys. Lett. **289**, 329-333 (1998).
[45] J. V. Zoval, J. Lee, S. Gorer, R. M. Penner, J. Phys. Chem. **102** (7), 1166-1175 (1998).
[46] F. Atamny, A. Baiker, Appl. Catal. A **173** (2), 201-230 (1998).
[47] S. J. Carroll, K. Seeger, R. E. Palmer, Appl. Phys. Lett. **72** (3), 305-307 (1998).
[48] R. Anton, I. Schneidereit, Phys. Rev. B **58** (20), 13874-13881 (1998).
[49] F. Gloaguen, G. M. Léger, C. Lamy, A. Marmann, U. Stimming, R. Voge, Electrochimica Acta **44**, 1805-1816 (1999).
[50] A. C. Hill, R. E. Patterson, J. P. Sefton, M. R. Columbia, Langmuir **15** (11), 4005-4010 (1999).
[51] F. Atamny, A. Baiker, Surf. Interface Anal. **27**, 512-516 (1999).
[52] C. Binns, S. H. Baker, C. Demangeat, J. C. Parlebas, Surf. Sci. Rep. **34**, 105-170 (1999).
[53] B. Blum, C. Salvarezza, J. Avria, J. Vac. Sci. Technol. B **17** (6), 2431-2438 (1999).
[54] K. Olaf, Ph.D. Thesis, Freie Univesität Berlin, Germany (1999).
[55] S. Štrbac, Z. Rakočević, K. I. Popov, M. G. Pavlović, R. Petrović, J. Serb. Chem. Soc. **64** (7-8), 483-493 (1999).

[56] A. R. Kucernak, P. B. Chowdhury, C. P. Wilde, G. H. Kelsall, Y. Y. Zhu, D. E. Williams, Electrochimica Acta **45**, 4483-4491 (2000).
[57] M. Aktary, C. E. Lee, Y. Xing, S. H. Bergens, M. T. McDermott, Lengmuir **16** (14), 5837-5840 (2000).
[58] W.-G. Lü, H. Wu, Y.-Q. Xiong, Y. Guo, D.-Q. Yang, and H.-L. Li, J. Vac. Sci. Technol. B **18** (3), 1156-1159 (2000).
[59] P. Shen, N. Chi, K.-Y. Chan, Appl. Surf. Sci. **172** (1-2), 159-166 (2001).
[60] D.-Q. Yang, E. Sacher, Surf. Sci. **516** (1-2), 43-55 (2002).
[61] B. Susla, R. Czajka, S. Szuba, M. Kaminski, T. Hihara, A. Kasuya, K. Sumiyama, Colloids and Surfaces A: Physicochemical and Engineering Aspects **202**, 187-193 (2002).
[62] B. Kaiser, B. Stegemann, H. Kaukel, K. Rademann, Surf. Sci. **496** (1-2), L18-L22 (2002).
[63] D.-L. Peng, G. Lerondel, T. Hihara, K. Sumiyama, T. Yao, Jpn. J. Appl. Phys. **41**, 5726-5729 (2002).
[64] O. V. Cherstiouk, P. A. Simonov, E. R. Savinova, Electrochimica Acta **48**, 3851-3860 (2003).
[65] R. Dolbec, E. Irissou, M. Chaker, D. Guay, F. Rosei, and M. A. El Khakani, Phys. Rev. B **70**, 201406(R) [4 pages] (2004).
[66] L. L. Wang. X. C. Ma, Y. Qi, P. Jiang, J. F. Jia, Q. K. Xue, J. Jiao, X. H. Bao, Ultramicroscopy **105**, 1-5 (2005).
[67] I. Lopez-Salido, D. Ch. Lim, Y. D. Kim, Surf. Sci. **588** (1-3), 6-18 (2005).
[68] D. Ch. Lim, I. Lopez-Salido, R. Dietsche, M. Bubek, Y. D. Kim, Surf. Sci. **600**, 507-513 (2006).
[69] I. L. Salido, Ph. D. Thesis, Universtität Konstanz, Germany (2007).
[70] D. Cattaneo, S. Foglio, C. S. Casari, A. Li Bassia, M. Passonia and C. E. Bottani, Surf. Sci. **601** (8), 1892-1897 (2007).
[71] E. Kadossov, J. Goering, U. Burghaus, Surf. Sci. **602** (3), 811-818 (2008).
[72] E. Kadossov, S. Funk, U. Burghaus, Catal. Lett. **120,** 179-183 (2008).
[73] M. Bayati, J. M. Abad, C. A. Bringes, M. J. Rosselinsky, D. J. Schiffrin, J. Electroanal. Chem. **623** (1), 19-28 (2008).
[74] T. Kondo, K. Izumi, K. Watahiki, Y. Iwasaki, T. Suzuki and J. Nakamura, J. Phys. Chem. C **112** (40), 15607-15610 (2008).
[75] J. Nakamura, T. Kondo, K. Watahiki, Y. Iwasaki, J. Pyo Oh, T. Suzuki, Y. Honma, D. Hatake, ECS Meeting, (San Francisco, California, 2009).
[76] H. Wolfschmidt, R. Busar, O. Paschos, T. Brulle, U. Stimming, 21st NAM, (San Francisco, California, 2009).
[77] H. Zhang, Q. Fu, Y. Yao, Z. Zhang, T. Ma, D. Tan and X. Bao, Langmuir **24**, 10874-10878 (2008).
[78] J. L. Rousset, A. M. Cadrot, F. J. C. Santos Aires, A. J. Renouprez, P. Mélinon, A. Perez, M. Pellarin, J. L. Vialle, and M. Broyer, J. Chem. Phys. **102** (21), 8574-8585 (1995).

[79] Y. Yao, Q. Fu, Z. Zhang, H. Zhang, T. Ma, D. Tan, X. Bao, Appl. Surf. Sci. **254** (13), 3808-3812 (2008).
[80] J. Plšek, P. Janda, Z. Bastl, Collect. Czech. Chem. Commun. **73**, 1299-1313 (2008).
[81] M. A. Vannice, J. E. Benson, M. Boudart, J. Catal. **16** (3), 273-416 (1970).
[82] N. E. Buyanova, A. P. Karnaukhov, N. H. Koroleva, Kinet. Katal. **26** (3), 741-748 (1975).
[83] D. J. O'Rear, D. G. Löffler, M. Boudart, J. Catal. **121** (1), 131-140 (1990).
[84] A. Guerrero-Ruiz, P. Badenes, I. Rodríguez-Ramos, Appl. Catal. A **173** (2), 313-321 (1998).
[85] M. A. Vannice, *Kinetics of catalytic reactions,* (Springer Science+Business Media, Inc., 2005).
[86] Y. Ji, A. M. J. van der Eerden, V. Koot, P. J. Kooyman, J. D. Meeldijk, B. M. Weckhuysen, D. C. Koningsberger, J. Catal. **234**, 376-384 (2005).
[87] P. Ferreira-Aparicio, Chem. Mater. **19** (24), 6030-6040 (2007).
[88] F. M. Hoffmann, J. Hrbek, R. A. Depaola, Chem. Phys. Lett. **106** (1-2), 83-86 (1984).
[89] M. Frank, R. Kühnemuth, M. Bäumer, H.-J. Freund, Surf. Sci. **454-456**, 968-973 (2000).
[90] J. Raskó, J. Catal. **217** (2), 478-486 (2001).
[91] R. G. Greenler, K. D. Burch, K. Kretzschmar, R. Klauser, A. M. Bradshaw, B. E. Hayden, Surf. Sci. **152** (1), 338-345 (1985).
[92] V. B. Kazansky, V. Yu. Borovkov, N. Sokolova, N. I. Jaeger, G. Schulz-Ekloff, Catal. Lett. **23**, 263-269 (1994).
[93] G. Rupprechter, T. Dellwig, H. Unterhalt, H.-J. Freund, J. Phys. Chem. B **105** (18), 3797-3802 (2001).
[94] P. Gruene, A. Fielicke, G. Meijer and D. M. Rayner, Phys. Chem. Chem. Phys. **10**, 6144-6149 (2008).
[95] K. McCrea, J. S. Parker, P. Chen, G. Somorjai, Surf. Sci. **494** (3), 238-250 (2001).
[96] Y. O. Park, W. F. Banholzer, R. I. Masel, Surf. Sci. **155** (1), 341-365 (1985).
[97] S. Tsuchiya, Y. Amenomiya, R. J. Cvetanović, J. Catal. **19** (3), 245-255 (1970).
[98] M. M. Goncharenko. V. V. Lobanov, P. E. Strizhak, Theor. Exper. Chem. **41** (5), 290-294 (2005).
[99] S. Vajda, M. J. Pellin, J. P. Greeley, C. L. Marshall, L. A. Curtiss, G. A. Ballentine, J. W. Elam, S. Catillon-Mucherie, P. C. Redfern, F. Mehmood, P. Zapol, Nature Materials **8**, 213-216 (2009).
[100] S. Vajda, M. J. Pellin, J. P. Greeley, C. L. Marshall, L. A. Curtiss, G. A. Ballentine, J. W. Elam, S. Catillon-Mucherie, P. C. Redfern, F. Mehmood, and P. Zapol, 21st NAM, (San Francisco, California, 2009).
[101] G.-W. Wu and K.-Y. Chan, J. Electroanal. Chem. **450**, 225-231 (1998).
[102] T. Li and P. B. Balbuena, J. Phys. Chem. B **105**, 9943-9952 (2001).

[103] Y. Xu, R. B. Getman, W. A. Shelton, W. F. Schneider, Phys. Chem. Chem. Phys. **10**, 6009-6018 (2008).
[104] G. Blyholder, J. Phys. Chem. **68** (10), 2772-2777 (1964).
[105] U. Heiz, R. Sherwood, D. M. Cox, A. Kaldor, J. T. Yates Jr., J. Phys. Chem. **99** (21), 8730-8735 (1995).
[106] G. Ganteför, G. S. Icking-Konert, H. Handschuh, W. Eberhardt, Int. J. Mass Spectrom. Ion Proc. **159** (1-3), 81-109 (1996).
[107] L. Wang, Chem. Phys. Lett. **443** (4-6), 304-308 (2007).
[108] Y. Yourdshahyan, V. R. Cooper, A. M. Kolpak, A. M. Rappe, Proc. SPIE **5223**, 223-31 (2004).
[109] C. Zhou, J. Wu, A. Nie, R. C. Forrey, A. Tachibana, H. Chen, J. Phys. Chem. C **111** (34), 12773-12778 (2007).
[110] M. K. Oudenhuijzen, Ph.D. Thesis, Utrecht University, The Netherlands (2002).
[111] W. T. Wallace, B. K. Min, D. W. Goodman, Top. Catal. **34** (1-4), (2005).
[112] I. P. Batra, N. Garcia, H. Rohrer, H. Salemink, E. Stoll, S. Ciraci, Surf. Sci. **181** (1-2), 126-138 (1987).
[113] P. Singjai, A. Zhdan, J. E. Castle, Philos. Mag. A **80** (10), 2445-2456 (2000).
[114] O. V. Sinitsyna, I. V. Yaminsky, Rus. Chem. Rev. **75** (1), 23-30 (2006).
[115] A. Rettenberger, P. Bruker, M. Metzler, F. Mugele, Th. W. Matthes, M. Böhmisch, J. Boneberg, K. Friemelt, P. Leiderer, Surf. Sci. **402-404**, 409-412 (1998).
[116] J. A. Venables, G. Haas, H. Brune, J. H. Harding, Mater. Res. Soc. Symp. Proc. **570**, 51 (1999).
[117] J. Dumont, F. Wiame, J. Ghijsen, R. Sporken. Surf. Sci. **572** (2-3), 459-466 (2004).
[118] H. Kawasaki, G. Sakai, T. Kijima, App. Surf. Sci. **253** (3), 1512-1516 (2006).
[119] W. B. Pearson, *Handbook of Lattice Spacings and Structures of Metals and Alloys,* (Pergamon Press, New York, 1958).
[120] J. H. Ryu, D. H. Seo, D. H. Kim, H. M Lee, Phys. Chem. Chem. Phys. **11**, 503-507 (2009).
[121] H. Groönbeck, P. Broqvist, J. Chem. Phys. **119** (7), 3896-3904 (2003).
[122] R. J. Good, L. A. Girifalco, G. Kraus, J. Phys. Chem. **62** (11), 1418-1421 (1958).
[123] F. R. de Boer, R. Boom, W. C. M. Mattens, A. R. Miedema and A. K. Niessen, *Cohesion and Structure,* Vol.1 (North-Holland, Amsterdam, 1988).
[124] S. Y. Liem, K. Y. Chan, Surf. Sci. **328** (1-2), 119-128 (1995).
[125] G.-W. Wu, K.-Y. Chan, Surf. Sci. **365** (1), 38-52, (1996).
[126] S. K. Nayak, P. Jena, V. S. Stepanyuk, W. Hergert, K. Wildberger, Phys. Rev. B **56**, 6952-6957 (1997).
[127] G. Rosenfeld, A. F. Becker, B. Poelsema, L. K. Verheij, G. Comsa, Phys. Rev. Lett. **69**, 917-920 (1992).
[128] J. Goniakowski, C. Motte, J. Cryst. Growth **275**, 29-38 (2005).

[129] Y. L. Wang. M. Y. Lai, J. Phys.: Condens. Matter **13**, R589-R618 (2001).
[130] S. Tsukamoto, N. Koguchi, J. Cryst. Growth **209**, 258-262 (2000).
[131] I.-S. Hwang, M-S. Ho, T. T. Tsong, Phys. Rev. Lett. **83**, 120-123 (1999).
[132] V. G. Kotlyar, A. V. Zotov, A. A. Saranin, T. V. Kasyanova, M. A. Cherevik, I. V. Pisarenko, V. G. Lifshits, Phys. Rev. B **66** (16), 165401 [4 pages] (2002).
[133] R. Kubo, A. Kawabata, S. Kobayashi, Annu. Rev. Mater. Sci. **14**, 49-66 (1984).
[134] P. Jena, A. W. Castleman, Jr., PNAS **103** (28), 10560-10569 (2006).
[135] X. Liu, M. Bauer, H. Bertagnolli, E. Roduner, J. van Slageren, F. Phillipp, Phys. Rev. Lett. **97**, 253401 [4 pages] (2006).
[136] S. Gan, Y. Liang, D. R. Baer, M. R. Sievers, G. S. Herman, and C. H. F. Peden, J. Phys. Chem. B **105** (12), 2412-2416 (2001).
[137] A. Bettac, L. Köller, V. Rank, K. H. Meiwes-Broer, Surf. Sci. **402-404**, 475-479 (1998).
[138] H. Tetsuichiro, Y. Hisato, K. Shini'ichi, K. Tamotsu, Nippon Kagakkai Koen Yokoshu **84** (1), 70 (2004).
[139] J. Chen, J. K.-Y.Chan, Mol. Sim. **31** (6-7), 527-533(7) (2005).
[140] S.-P. Huang, P. B. Balbuena, Mol. Phys. **100** (13), 2165-2174 (2002).
[141] K. Okazaki-Maeda, Y. Morikawa, S. Tanaka, M. Kohyama, Mater. Res. Soc. Symp. Proc. 900E O06-35 (2005).
[142] K. Okazaki-Maeda, S. Yamakawa, Y. Morikawa, T. Akita, S. Tanaka, S. Hyodo, M. Kohyama, J. Phys.: Conf. Ser. **100** (7), 072044 (2008).
[143] H. Häkkinen, S. Abbet, A. Sanchez, U. Heiz, U. Landman, Angew. Chem., Int. Ed. **42**, 1297-1300 (2003).
[144] A-C. Shi, R. I. Masel, J. Catal. **120** (2), 421-431 (1989).
[145] J. T. Miller, B. L. Meyers, F. S. Modica, G. S. Lane, M. Vaarkamp, D. C. Koningsberger, J. Catal. **143** (2), 395-408 (1993).
[146] P. J. F. Harris, Int. Mater. Rev. **40**, 97-115 (1995).
[147J. W. Arblaster, Plat. Met. Rev. **49** (3), 141-149 (2005).
[148] X. Lin, N. J. Ramer, A. M. Rappe, K. C. Hass, W. F. Schneider, B. L. Trout, J. Phys. Chem. B **105**, 7739-7747 (2001).
[149] X. Lai, T. P. St. Clair, D. W. Goodman, Faraday Discuss. **144**, 279-284 (1999).
[150] E. I. Altman and R. J. Gorte, Surf. Sci. **172** (1), 71-80 (1986).
[151] A. Berkó, J. Szök, F. Solymosi, Surf. Sci. **566-568**, 337-342 (2004).
[152] E. S. Putna, J. M. Vohs, R. J. Gorte, Surf. Sci. **391** (1-3), L1178-L1182 (1997).
[153] N. I. Jaeger, A. L. Jourdan and G. Schulz-Ekloff, J. Chem. Soc., Faraday Trans. **87**, 1251-1257 (1991).
[154] P. Denton, A. Giroir-Fendler, H. Praliaud, M. Primet, Top. Catal. **16/17** (1-4), 377-380 (2001).
[155] Nicola Seriani, Ph. D. Thesis, Technische Universität Dresden, Germany (2006).
[156] P. Wynblatt, Acta Metallurgica **24** (12), 1175-1182 (1976).

[157] J. M. Rickard, L. Genovese, A. Moata, S. Nitsche, J. Catal. **121** (1), 141-152 (1990).
[158] C. G. Granqvist, R. A. Buhrman, J. Catal. **42** (3), 477-479 (1976).
[159] M. J. J. Jak, Ph. D. Thesis, Leiden University, The Netherlands (2000).
[160] A. K. Datye, Q. Xu, K. C. Kharas, J. M. McCarty, Catal. Today **111,** 59-67 (2006).
[161] D. Kandel, Phys. Rev. Lett. **79** (21), 4238-4241 (1997).
[162] M. von Smoluchowski, Phys. Z. **17**, 557-585 (1916).
[163] B. K. Chakraverty, J. Phys. Chem. Solids **28**, 2401-2412 (1967).
[164] G. A. Fuentes, E. Salinas-Rodriguez, Studies Surf. Sci. Catal. **139**, 503-510 (2001).
[165] M. Conti, B. Meerson, A. Peleg and P. V. Sasorov, Phys. Rev. E **65**, 046117 (2002).
[166] W. D. Luedtke, U. Landman, Phys. Rev. Lett. **82** (19), 3835-3838 (1999).
[167] B. Yoon, W. D. Luedtke, J. Gao, U. Landman, J. Phys. Chem. B **107** (24), 5882-5891 (2003).
[168] W. H. Lee, K. R. Vanloon, V. Petrova, J. B. Woodhouse, C. M. Loxton, R. I. Masel, J. Catal. **126** (2), 658-671 (1990).
[169] H. Graoui, S. Giorgio, C. R. Henry, Surf. Sci. **417** (2-3), 350-360 (1998).
[170] U. Heiz, A. Sanchez, S. Abbet, W.-D. Schneider, ISSPIC **9**, (Lausanne, 1998).
[171] Y. Shi, K. M. Ervin, J. Chem. Phys. **108** (5), 1757 (1998).
[172] U. Heiz, A. Sanchez, S. Abbet, W.-D. Schneider, J. Am. Chem. Soc. **121**, 3214-3217 (1999).
[173] A. Eichler, Phys. Rev. B **71**, 125418 [8 pages] (2005).